
Resisting Adversarial Attacks by k -Winners-Take-All

Chang Xiao Peilin Zhong Changxi Zheng
 Columbia University
 {chang, peilin, cxz}@cs.columbia.edu

Abstract

We propose a simple change to the current neural network structure for defending against gradient-based adversarial attacks. Instead of using popular activation functions (such as ReLU), we advocate the use of k -Winners-Take-All (k -WTA) activation, a C^0 discontinuous function that purposely invalidates the neural network model’s gradient at densely distributed input data points. Our proposal is theoretically rationalized. We show why the discontinuities in k -WTA networks can largely prevent gradient-based search of adversarial examples and why they at the same time remain innocuous to the network training. This understanding is also empirically backed. Even without notoriously expensive adversarial training, the robustness performance of our networks is comparable to conventional ReLU networks optimized by adversarial training. Furthermore, after also optimized through adversarial training, our networks outperform the state-of-the-art methods under white-box attacks on various datasets that we experimented with.

1 Introduction

In the tremendous success of deep learning techniques, there is a grain of salt. It has become well-known that deep neural networks can be easily fooled by *adversarial examples* [1]. Those deliberately crafted input samples can mislead the networks to produce an output drastically different from what we expect. In many important applications, from face recognition authorization to autonomous cars, this vulnerability gives rise to serious security concerns [2, 3, 4, 5].

Attacking the network is straightforward. Provided a labeled data item (x, y) , the attacker finds a perturbation x' imperceptibly similar to x but misleading enough to cause the network to output a label different from y . By far, the most effective way of finding such a perturbation (or adversarial example) is by exploiting the gradient information of the network with respect to its input; the gradient indicates how to perturb x to trigger the maximal change of y .

The defense, however, is challenging. Recent studies showed that adversarial examples always exist if one tends to pursue a high classification accuracy—adversarial robustness seems at odds with the accuracy [6, 7, 8, 9]. This intrinsic difficulty of eliminating adversarial examples suggests an alternative path: *can we design a network whose adversarial examples are evasive rather than eliminated?* Indeed, along with this thought is a series of works using obfuscated gradient as a defense mechanism [10]. Those methods hide the network’s gradient information by artificially discretizing the input [11, 12] or introducing certain randomness to the input [13, 14] or the network structure [15, 16] (more discussion in Sec. 1.1). Yet, the hidden gradient in those methods can still be approximated, and as recently pointed out in [10], those methods remain vulnerable.

Technical contributions. Rather than obfuscating the network’s gradient, we make the gradient *undefined*. This is achieved by a simple change to the standard neural network structure: we advocate the use of a C^0 discontinuous activation function, namely the k -Winners-Take-All (k -WTA) activation, to replace the popular activation functions such as rectified linear units (ReLU). This is the only change we propose to a deep neural network, and all other components (such as BatchNorm, convolution, pooling) remain unaltered.

k -WTA activation takes as input the entire output of a layer, retains its k largest values and deactivates all others to zero. As we will show in this paper, even an infinitesimal change to the input may cause a complete change to the network neurons’ activation pattern, thereby resulting in a large jump in the

network’s output. This means that, mathematically, if we use $f(\mathbf{x}; \mathbf{w})$ to denote a k -WTA network taking an input \mathbf{x} and parameterized by weights \mathbf{w} , then the gradient $\nabla_{\mathbf{x}} f(\mathbf{x}; \mathbf{w})$ at certain \mathbf{x} is undefined— $f(\mathbf{x}; \mathbf{w})$ is C^0 discontinuous.

More intriguing than the mere replacement of the activation function is *why k -WTA helps improve the adversarial robustness*. We offer our theoretical reasoning of its behavior from two perspectives. On the one hand, we show that the discontinuities of $f(\mathbf{x}; \mathbf{w})$ is *densely distributed* in the space of \mathbf{x} . Dense enough such that a tiny perturbation from any \mathbf{x} almost always comes across some discontinuities, where the gradients are undefined and thus the attacker’s search of adversarial examples becomes blinded (see Figure 1 for a 1D illustration).

On the other hand, there seems to be a paradox. The discontinuities in the activation function also renders $f(\mathbf{x}, \mathbf{w})$ discontinuous with respect to the network weights \mathbf{w} (at certain \mathbf{w} values). But training the network relies on a presumption that the gradient with respect to the weights is (almost) always available. Interestingly, under k -WTA activation, the discontinuities of $f(\mathbf{x}, \mathbf{w})$ is rather *sparse* in the space of \mathbf{w} , intuitively because the dimension of \mathbf{w} (in parameter space) is much larger than the dimension of \mathbf{x} (in data space). Thereby, the network can be trained successfully.

Summary of results. In addition to the theoretical analysis, we conducted extensive experiments, on various datasets (including MNIST, CIFAR, and SVHN), under different network architectures (including ResNet [17], DenseNet [18], and Wide ResNet [19]), and against a diverse set of attack methods (including PGD [20], Deepfool [21], C&W [22], and others).

In comparison to ReLU networks, k -WTA networks have clearly improved robustness against gradient-based attacks. Under a mild perturbation, even without adversarial training, our networks’ robustness is comparable to ReLU networks optimized by adversarial training. This is a remarkable advantage, as adversarial training is notoriously expensive (typically 10-20 \times slower than the regular training). Furthermore, after also optimized through adversarial training, our networks outperform the state-of-the-art methods under white-box attacks on all three datasets that we experimented with.

To promote reproducible research, we release our implementation of k -WTA networks, along with all our experiment code, configuration files and pre-trained models.¹

1.1 Related Work: Obfuscated Gradient as a Defense Mechanism

Before delving into k -WTA details, we review prior adversarial defense methods that share the same philosophy with us and highlight our advantages. For a review of other attack and defense methods, we refer to Appendix A.

Methods aiming for concealing the gradient information from the attacker has been termed as *obfuscated gradient* [10] or *gradient masking* [23, 24] techniques. One type of such methods is by exploiting randomness, either randomly transforming the input before feeding it to the network [13, 14] or introducing stochastic layers in the network [15]. However, the gradient information in these methods can be estimated by taking the average over multiple trials [10, 25]. As a result, these methods are vulnerable.

Another type of obfuscated gradient methods relies on the so-called *shattered gradient* [10], which aims to make the network gradients nonexistent or incorrect to the attacker, by purposely discretizing the input [11, 26] or artificially raising numerical instability for gradient evaluation [27, 28]. Unfortunately, these methods are also vulnerable. As shown by Athalye et al. [10], they can be compromised by *backward pass differentiable approximation* (BPDA). Suppose $f_i(\mathbf{x})$ is a non-differentiable component of a network expressed by $f = f_1 \circ f_2 \circ \dots \circ f_n$. The gradient $\nabla_{\mathbf{x}} f$ can be estimated as long as one can find a smooth delegate g that approximates well f_i (i.e., $g(\mathbf{x}) \approx f_i(\mathbf{x})$).

In stark contrast to all those methods, our use of k -WTA activation is not just meant to obfuscate the network’s gradients but to destroy them at certain input samples. More importantly, those discontinuities are densely distributed in the input data space, and a slight change of the activation pattern in an earlier layer of the network can cause a radical reorganization of activation patterns in

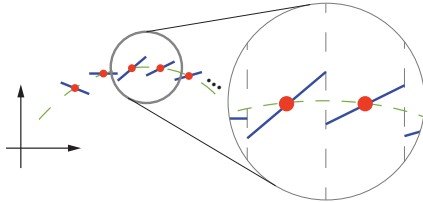


Figure 1: Fit a 1D function (green curve) using a k -WTA model provided with a set of points (red). The resulting model is piecewise continuous (blue), and the discontinuities can be dense.

¹<https://github.com/a554b554/kWTA-Activation.git>.

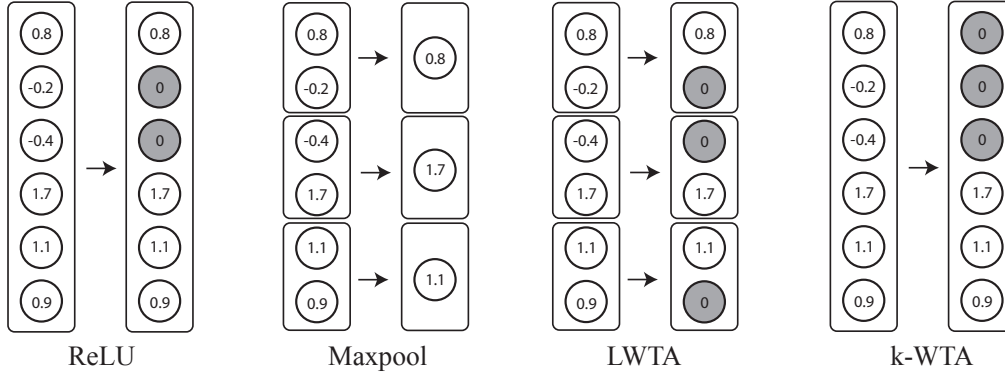


Figure 2: **Different activation functions.** **ReLU:** all neurons with negative activation values will be set to zero. **Max-pooling:** only the largest activation in each group is transmitted to the next layer, and this effectively downsample the output. **LWTA:** the largest activation in each group retains its value when entering the next layer, others are set to zero. **k -WTA:** the k largest activations in the entire layer retain their values when entering the next layer, others are set to zero ($k = 3$ in this example). Note that the output is not downsampled through ReLU, LWTA and k -WTA.

later layers. To our knowledge, it is extremely hard, if not impossible, to effectively approximate a k -WTA network using a smooth function. Thus, BPDA attacks can be prevented.

2 k -Winners-Take-All Activation

The debut of the *Winner-Takes-All* (WTA) activation on the stage of neural networks dates back to 1980s, when Grossberg [29] introduced shunting short-term memory equations in on-center off-surround networks and showed the ability to identify the largest of N real numbers. Later, Majani et al. [30] generalized the WTA network to identify the K largest of N real numbers, and they termed the network as the K -Winners-Take-All (KWTA) network. These early WTA-type activation functions output only boolean values, mainly motivated by the properties of biological neural circuits. In particular, Maass [31, 32] has proved that any boolean function can be computed by a single KWTA unit. Yet, the boolean nature of these activation functions differs starkly from the modern activation functions, including the one we will use.

2.1 Deep Neural Networks Activated by k -Winners-Take-All

We propose to use k -Winners-Take-All (k -WTA) activation, a natural generalization of the boolean KWTA² [30]. k -WTA retains the k largest values of an $N \times 1$ input vector and sets all others to be zero before feeding the vector to the next network layer, namely,

$$\phi_k(\mathbf{y})_j = \begin{cases} y_j, & y_j \in \{k \text{ largest elements of } \mathbf{y}\}, \\ 0, & \text{Otherwise.} \end{cases} \quad (1)$$

Here $\phi_k : \mathbb{R}^N \rightarrow \mathbb{R}^N$ is the k -WTA function (parameterized by an integer k), $\mathbf{y} \in \mathbb{R}^N$ is the input to the activation, and $\phi_k(\mathbf{y})_j$ denote the j -th element of the output $\phi_k(\mathbf{y})$ (see the rightmost subfigure of Figure 2). Note that if \mathbf{y} has multiple elements that are equally k -th largest, we break the tie by retaining the element with smaller indices until the k slots are taken.

When using k -WTA activation, we need to choose k . Yet it makes no sense to fix k throughout all layers of the neural network, because these layers often have different output dimensions; a small k to one layer’s dimension can be relatively large to the other. Instead of specifying k , we introduce a parameter $\gamma \in (0, 1)$ called *sparsity ratio*. If a layer has an output dimension N , then its k -WTA activation has $k = \lfloor \gamma \cdot N \rfloor$. Even though the sparsity ratio can be set differently for different layers, in practice we found no clear gain from introducing such a variation. Therefore, we use a fixed γ —the only additional hyperparameter needed for the neural network.

In convolutional neural networks (CNN), the output of a layer is a $C \times H \times W$ tensor. C denotes the number of output channels; H and W indicate the feature resolution. While there are multiple choices of applying k -WTA on the tensor—for example, one can apply k -WTA individually to each

²In this paper, we use k -WTA to refer our activation function, while using KWTA to refer the original boolean version by Majani et al. [30].

channel—empirically we found that the most effective (and conceptually the simplest) way is to treat the tensor as a long $C \cdot H \cdot W \times 1$ vector input to the k -WTA activation. Using k -WTA in this way is also backed by our theoretical understanding (see Sec. 3).

k -WTA activation has a $O(N \log N)$ complexity since it needs to sort input values. While this is slightly more expensive than ReLU’s $O(N)$ cost, this activation overhead is negligible in comparison to the matrix multiplication cost, which is a neural network’s performance bottleneck.

Remark: difference from other WTA-type activations. Relevant to k -WTA is the *local Winner-Take-All* (LWTA) activation (by Srivastava et al. [33, 34]), which divides output values of a layer into local groups and applies WTA to each group of values. LWTA is similar to max-pooling [35] for dividing the layer output and choosing group maximums. But unlike ReLU and max-pooling being C^0 continuous, LWTA and our k -WTA are both discontinuous with respect to the input. The differences among ReLU, max-pooling, LWTA, and our k -WTA are illustrated in Figure 2.

LWTA is motivated toward preventing catastrophic forgetting [36], whereas our use of k -WTA is for defending against adversarial threat. While both are discontinuous, it remains unclear what the LWTA’s discontinuity properties are and how its discontinuities affect the network training. Our theoretical analysis (Sec. 3), in contrast, sheds some light on these fundamental questions about k -WTA, rationalizing its use for improving adversarial robustness. Indeed, our early experiments also confirmed that k -WTA outperforms LWTA in terms of robustness.

WTA-type activation in general, albeit originated decades ago, remains elusive in modern neural networks. Perhaps this is because it has not demonstrated a considerable improvement to the network’s standard test accuracy (though it can offer an accuracy comparable to ReLU [33]). Our analysis and proposed use of k -WTA and its enabled improvement in the context of adversarial defense may suggest a renaissance of studying WTA.

2.2 Training k -WTA Networks

k -WTA networks require no special treatment in training. Any optimization algorithm (such as stochastic gradient descent) for training ReLU networks can be directly used to train k -WTA networks.

Our experiments have found that when the sparsity ratio γ is relatively small (≤ 0.2), the network training converges slowly. This is not a surprise. A smaller γ activates fewer neurons, effectively reducing more of the layer width and in turn the network size, and the stripped “subnetwork” is much less expressive [33]. Since different training examples activate different subnetworks, collectively they make the training harder.

Nevertheless, we prefer a smaller γ . As we will discuss in the next section, a smaller γ usually leads to better robustness against finding adversarial examples. Therefore, to ease the training (when γ is small), we propose to use an iterative fine-tuning approach. Suppose the target sparsity ratio is γ_1 . We first train the network with a larger sparsity ratio γ_0 using the standard training process. Then, we iteratively fine tune the network. In each iteration, we reduce its sparsity ratio by a small δ and train the network for two epochs. The iteration repeats until γ_0 is reduced to γ_1 .

This incremental process introduces little training overhead, because the cost of each fine tuning is negligible in comparison to training from scratch toward γ_0 . We also note that this process is optional. In practice we use it only when $\gamma < 0.2$.

3 Understanding k -WTA Discontinuity

We now present our theoretical understanding of k -WTA’s discontinuity behavior in the context of deep neural networks, revealing some implication toward the network’s adversarial robustness.

Activation pattern. To understand k -WTA’s discontinuity, consider one layer outputting values \mathbf{x} , passed through a k -WTA activation, and followed by the next layer whose linear weight matrix is W (see adjacent figure). Then, the value fed into the next activation can be expressed as $W\phi_k(\mathbf{x})$, where $\phi_k(\cdot)$ is the k -WTA function defined in (1). Suppose the vector \mathbf{x} has a length l . We define the k -WTA’s *activation pattern* under the input \mathbf{x} as



$$\mathcal{A}(\mathbf{x}) := \{i \in [l] \mid x_i \text{ is one of the } k \text{ largest values in } \mathbf{x}\} \subseteq [l]. \quad (2)$$

Here (and throughout this paper), we use $[l]$ to denote the integer set $\{1, 2, \dots, l\}$.

Discontinuity. The activation pattern $\mathcal{A}(\mathbf{x})$ is a key notion for analyzing k -WTA’s discontinuity behavior. Even an infinitesimal perturbation of \mathbf{x} may change $\mathcal{A}(\mathbf{x})$: some element i is removed

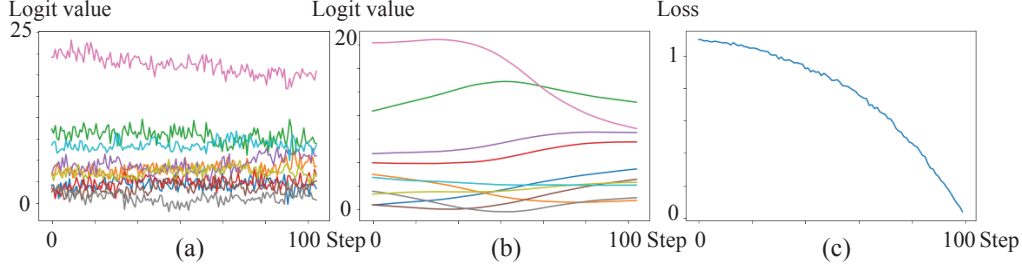


Figure 3: **(a, b)** We plot the change of 10 logits values when conducting untargeted PGD attack with 100 iterations. X-axis indicates the perturbation size ϵ and Y-axis indicates the 10 color-coded logits values. **(a)** When we apply PGD attack on k -WTA ResNet18, the strong discontinuities w.r.t. to input invalidate gradient estimation, effectively defending well against the attack. **(b)** In contrast, for a ReLU ResNet18, PGD attack can easily find adversarial examples due to the model’s smooth change w.r.t. input. **(c)** In the process of training k -WTA ResNet18, the loss change w.r.t. model weights is largely smooth. Thus, the training is not harmed by k -WTA’s discontinuities.

from $\mathcal{A}(\mathbf{x})$ while another element j is added in. Corresponding to this change, in the evaluation of $W\phi_k(\mathbf{x})$, the contribution of W ’s column vector W_i vanishes while another column W_j suddenly takes effect. It is this abrupt change that renders the result of $W\phi_k(\mathbf{x})$ C^0 discontinuous.

Such a discontinuity jump can be arbitrarily large, because the column vectors W_i and W_j can be of any difference. Once W is determined, the discontinuity jump then depends on the value of x_i and x_j . As explained in Appendix C, when the discontinuity occurs, x_i and x_j have about the same value, depending on the choice of the sparsity ratio γ (recall Sec. 2.1)—the smaller the γ is, the larger the jump will be. This relationship suggests that a smaller γ will make the search of adversarial examples harder. Indeed, this is confirmed through our experiments (see Appendix B.6).

Piecewise linearity. Now, consider an n -layer k -WTA network, which can be expressed as $f(\mathbf{x}) = W^{(1)} \cdot \phi_k(W^{(2)} \cdot \phi_k(\dots \phi_k(W^{(n)} \mathbf{x} + \mathbf{b}^{(n)})) + \mathbf{b}^{(2)}) + \mathbf{b}^{(1)}$, where $W^{(i)}$ and $\mathbf{b}^{(i)}$ are the i -th layer’s weight matrix and bias vector, respectively. If the activation patterns of all layers are determined, then $f(\mathbf{x})$ is a linear function. When the activation pattern changes, $f(\mathbf{x})$ switches from one linear function to another linear function. Over the entire space of \mathbf{x} , $f(\mathbf{x})$ is *piecewise* linear. The set of activation patterns of all layers defines a specific linear piece of the function, or a *linear region* (following the notion introduced by Montufar et al. [37]). Conventional ReLU (or hard tanh) networks also represent piecewise linear functions and their linear regions are joined together at their boundaries, whereas in k -WTA networks the linear regions are disconnected (see Figure 1).

Linear region density. Next, we gain some insight on the distribution of those linear regions. This is of our interest because if the linear regions are densely distributed, a small $\Delta\mathbf{x}$ perturbation from any data point \mathbf{x} will likely cross the boundary of the linear region where \mathbf{x} locates. Whenever boundary crossing occurs, the gradient becomes undefined (see Figure 3-a).

For the purpose of analysis, consider an input \mathbf{x} passing through a layer followed by a k -WTA activation (see adjacent figure). The output from the activation is $\phi_k(W\mathbf{x} + \mathbf{b})$. We would like to understand, when \mathbf{x} is changed into \mathbf{x}' , how likely the activation pattern of ϕ_k will change. First, notice that if \mathbf{x}' and \mathbf{x} satisfy $\mathbf{x}' = c \cdot \mathbf{x}$ with some $c > 0$, the activation pattern remains unchanged. Therefore, we introduce a notation $d(\mathbf{x}, \mathbf{x}')$ that measures the “perpendicular” distance between \mathbf{x} and \mathbf{x}' , one that satisfies $\mathbf{x}' = c \cdot (\mathbf{x} + d(\mathbf{x}, \mathbf{x}')\mathbf{x}_\perp)$ for some scalar c , where \mathbf{x}_\perp is a unit vector perpendicular to \mathbf{x} and on the plane spanned by \mathbf{x} and \mathbf{x}' . With this notion, and if the elements in W is initialized by sampling from $\mathcal{N}(0, \frac{1}{l})$ and \mathbf{b} is initialized as zero, we find the following property:



Theorem 1 (Dense discontinuities). *Given any input $\mathbf{x} \in \mathbb{R}^m$ and some β , and $\forall \mathbf{x}' \in \mathbb{R}^m$ such that $\frac{d^2(\mathbf{x}, \mathbf{x}')}{\|\mathbf{x}\|_2^2} \geq \beta$, if the following condition*

$$l \geq \Omega \left(\left(\frac{m}{\gamma} \cdot \frac{1}{\beta} \right) \cdot \log \left(\frac{m}{\gamma} \cdot \frac{1}{\beta} \right) \right)$$

is satisfied, then with a probability at least $1 - \cdot 2^{-m}$, we have $\mathcal{A}(W\mathbf{x} + \mathbf{b}) \neq \mathcal{A}(W\mathbf{x}' + \mathbf{b})$.

Here l is the width of the layer, and γ is, as before, the sparsity ratio in k -WTA. This theorem informs us that the larger the layer width l is, the smaller β —and thus the smaller perpendicular perturbation

Activation	model	a_{std}	$A_{rob}(\epsilon = 1)$	$A_{rob}(\epsilon = 2)$	$A_{rob}(\epsilon = 4)$	$A_{rob}(\epsilon = 8)$
ReLU	WRN	91.0%	10.1%	0.8%	0.0%	0.0%
	WRN+adv	83.3%	80.0%	75.6%	66.2%	43.1%
	WRN+TRADE	78.9%	76.2%	71.9%	65.8%	50.1%
k -WTA	WRN-0.1	88.6%	74.6%	57.7%	36.0%	22.5%
	WRN-0.1+adv	73.8%	71.4%	70.0%	66.8%	59.3%

Table 1: Wide Resnet(WRN) on CIFAR with different perturbation sizes. WRN-0.1 indicates WRN model with k -WTA activation of sparsity $\gamma = 0.1$ (without adversarial training); +adv indicates models with adversarial training; +TRADE indicates models trained with TRADE.

distance $d(\mathbf{x}, \mathbf{x}')$ —is needed to trigger a change of the activation pattern, that is, as the layer width increases, the piecewise linear regions become finer (see Appendix D for the theorem proof and more discussion). This property also echos a similar trend in ReLU networks, as pointed out in [38].

Why is the k -WTA network trainable? While k -WTA networks are highly discontinuous as revealed by Theorem 1 and our experiments (Figure 3-a), in practice we experience no difficulty on training these networks. Our next theorem sheds some light on the reason behind the training success.

Theorem 2. Consider N data points $\mathbf{x}_1, \mathbf{x}_2, \dots, \mathbf{x}_N \in \mathbb{R}^m$. Suppose $\forall i \neq j, \frac{\mathbf{x}_i}{\|\mathbf{x}_i\|_2} \neq \frac{\mathbf{x}_j}{\|\mathbf{x}_j\|_2}$. If l is sufficiently large, then with a high probability, we have $\forall i \neq j, \mathcal{A}(W\mathbf{x}_i + \mathbf{b}) \cap \mathcal{A}(W\mathbf{x}_j + \mathbf{b}) = \emptyset$.

This theorem is more formally stated in Theorem 10 in Appendix D together with a proof there. Intuitively speaking, it states that if the network is sufficiently wide, then for any $i \neq j$, activation pattern of input data \mathbf{x}_i is almost separated from that of \mathbf{x}_j . Thus, the weights for predicting \mathbf{x}_i 's and \mathbf{x}_j 's labels can be optimized almost independently, without changing their individual activation patterns. In practice, the activation patterns of \mathbf{x}_i and \mathbf{x}_j are not fully separated but weakly correlated. During the optimization, the activation pattern of a data point \mathbf{x}_i may change, but the chance is relatively low—a similar behavior has also been found in ReLU networks [39].

Further, notice that the training loss takes a summation over all training data points. This means a weight update would change only a small set of activation patterns (since the chance of having the pattern changed is low); the discontinuous change on the loss value, after taking the summation, will be negligible (see Figure 3-c). Thus, the discontinuities in k -WTA is not harmful to network training.

4 Experimental Results

We now evaluate the k -WTA network under various types of adversarial attacks and compare it with other defense methods. When reporting statistics, we use A_{rob} to indicate the model accuracy under adversarial attacks applied to the test dataset, and A_{std} to indicate the accuracy on the clean test data.

4.1 Gradient-Based Attack

We evaluate our method on three datasets, MNIST [40], CIFAR-10 [41] and SVHN [42], since they have been extensively used in previous research for evaluating adversarial robustness.

CIFAR-10. On CIFAR-10, we use untargeted *Projected Gradient Descent* (PGD) attack [20] (with random initialization for 20 iterations) to find adversarial examples that perturb image pixels (in the range of [0, 255]) within an ℓ_∞ ϵ -ball. We test four perturbation ranges, with $\epsilon = 1, 2, 4, 8$ in terms of pixel values. Before feeding the images to the network, we normalize them into [0, 1].

In Table 1, we report the results on Wide ResNet (WRN) [19] with depth 22 and widen factor 10 (WRN-22-10). We compare our method with adversarial training [43] and TRADE [7]; both are considered the state-of-the-art defense against white-box gradient-based attacks. Here we use the parameter $1/\lambda = 6$ in TRADE, a value that leads to the best robustness according to their paper.

The ReLU networks in our tests are trained with stochastic gradient descent (SGD) with momentum=0.9. we using a learning rate 0.1 from 1 to 60 epochs, 0.01 during 60-80 epochs and 0.001 during 80-100 epochs. k -WTA networks, without adversarial training, are trained incrementally, starting with $\gamma = 0.2$ for 60 epochs with SGD (learning rate=0.1, momentum=0.9) and then decreasing γ by 0.005 every 2 epochs until γ reaches the desired value. When adversarial training is used, the k -WTA networks are trained in the same way as ReLU networks, without fine-tuning.

As shown in Table 1, when $\epsilon = 1$, WRN-22-10 with k -WTA ($\gamma=0.1$) activation, even without adversarial training, achieves a robust accuracy (A_{rob}) comparable to the ReLU model optimized with adversarial training. Meanwhile, ReLU model without adversarial training can be easily attacked by adversarial examples. As ϵ increases, the accuracy A_{rob} of the k -WTA model starts to drop.

Activation	MNIST model	a_{std}	A_{rob}	SVHN Model	A_{std}	A_{rob}
ReLU	CNN	99.4%	0.0%	ResNet18	95.0%	0.0%
	CNN+adv	99.2%	95.0%	ResNet18+adv	84.2%	44.5%
	CNN+TRADE	99.2%	96.0%	ResNet18+TRADE	87.6%	42.4%
k -WTA	CNN-0.08	99.3%	62.2%	ResNet18-0.1	89.3%	12.1%
	CNN-0.08+adv	99.20%	96.4%	ResNet18-0.1+adv	83.5%	73.4%

Table 2: Results on MNIST and SVHN datasets. +adv indicates models with adversarial training; +TRADE indicates models trained with TRADE

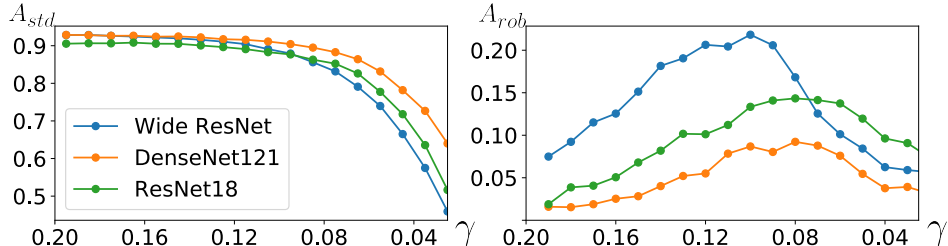


Figure 4: Robustness changing w.r.t. γ on CIFAR. When γ decreases, the standard test accuracy (left) starts to drop after a certain point. The robust accuracy (right) first increases then decreases.

However, when adversarial training is employed to train the k -WTA network, it outperforms the ReLU networks with both adversarial training and TRADE.

The advantages of k -WTA networks consistently retain on other architectures (including ResNet [17], DenseNet [18]) and against different attack methods (e.g., C&W attack [22], Deepfool [21]). Please refer to Appendix B.2 and Appendix B.3 for details.

MNIST and SVHN. On MNIST and SVHN datasets, we test our model with perturbation size $\epsilon=0.3$ and $\epsilon=0.047$, respectively, for pixel values ranged in $[0, 1]$. The robust accuracy are evaluated under PGD attacks with random initialization for 20 iterations, and the results are summarized in Table 2 and Appendix B.2.

When testing on MNIST dataset, we use a 4-layer convolutional network trained by SGD with a learning rate 0.01 for 20 epochs. The CNN architecture details are provided in Appendix B.7, and the k -WTA CNNs in our test are all trained from scratch without incremental fine-tuning. On SVHN dataset, we use standard ResNet18 and the same optimization protocol as what we used on CIFAR. Even without adversarial training, the k -WTA model already performs slightly better than the ReLU model. After using adversarial training, the k -WTA model outperforms considerably the adversarially trained ReLU model. Especially on SVHN dataset, the accuracy is boosted from 44.5% to 73.4%.

Varying sparsity ratio γ and model architecture. We further evaluate our method on various network architectures with different sparsity ratios γ . Figure 4 shows the standard test accuracies and robust accuracies against PGD attacks while γ decreases. To test against different network architectures, we apply k -WTA to ResNet18, DenseNet121 and Wide ResNet (WRN-22-12). In each case, starting from $\gamma = 0.2$, we decrease γ using incremental fine-tuning. We then evaluate the robust accuracy on CIFAR dataset, taking 20-iteration PGD attacks with a perturbation range $\epsilon = 8$ for pixels ranged in $[0, 255]$.

We find that when γ is larger than ~ 0.1 , reducing γ has little effect on the standard accuracy, but increases the robust accuracy. When γ is smaller than ~ 0.1 , reducing γ drastically lowers both the standard and robust accuracies. The peaks in the A_{rob} curves (Figure 4-right) are consistent with our theoretical understanding: Theorem 1 suggests that when l is fixed, a smaller γ tends to sparsify the linear region boundaries, exposing more gradients to the attacker. Meanwhile, as also discussed in Sec. 3, a smaller γ leads to a larger discontinuity jump and thus tends to improve the robustness.

4.2 Black-Box Attack

Next, we evaluate the robustness of k -WTA models under black-box attacks. Note that the use of k -WTA is motivated for defending against gradient-based attacks; it is not specifically designed for defending under black-box attacks. Regardless, we find that k -WTA models still have better robust accuracies than ReLU models, although with adversarial training k -WTA models do not show better performance in comparison to adversarially trained ReLU models. However, when both k -WTA and ReLU models are trained on clean data without adversarial training, k -WTA models (such as ResNet18-0.08) defend much better against black-box attacks. The results are reported in Table 3.

Activation	Model	A_{rob}	A_{std}	Model	A_{rob}	A_{std}
ReLU	ResNet18	5.9%	90.9%	DenseNet121	6.6%	91.1%
k -WTA	ResNet18-0.18	41.9%	90.6%	DenseNet121-0.18	26.5%	92.6%
k -WTA	ResNet18-0.13	45.6%	89.7%	DenseNet121-0.13	32.1%	91.7%
k -WTA	ResNet18-0.08	50.1%	86.1%	DenseNet121-0.08	37.3%	89.5%

Table 3: Results on black box attack.

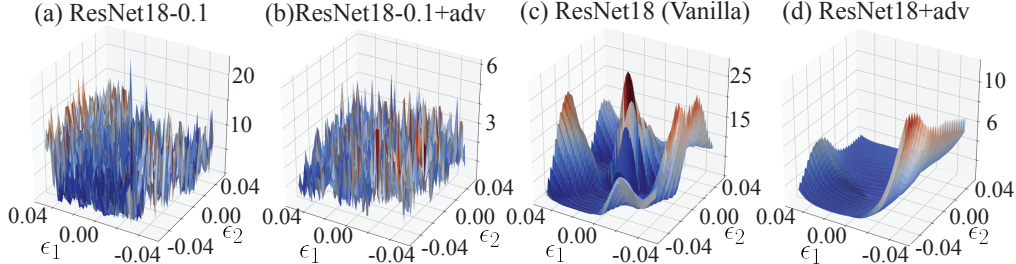


Figure 5: Gradient-based attack’s loss landscapes in k -WTA (**a**, **b**) and conventional ReLU models (**c**, **d**). (a,b) k -WTA Models have much more non-convex and non-smooth landscapes. Also, the model optimized by adversarial training (b) has a lower absolute value of loss.

So far the most effective black-box attack is transfer attack [23, 24], based on the observations that adversarial examples identified in one network are likely to fool other networks trained for the same task. To evaluate our models, we use ResNet18 trained on clean CIFAR-10 dataset as the source model to transfer attack our models. As shown in Table 3, k -WTA models produce better robust accuracies than ReLU models under transfer attacks. The robustness-accuracy trade-off [6] can be also seen in the black-box attack scenario: as γ is reduced, the standard accuracy of the k -WTA model will decrease but its robust accuracy increases. In addition, we find that when γ is relatively large, k -WTA models achieve similar (sometimes even better) standard accuracies than ReLU models, while maintaining better robustness. This suggests that k -WTA can be a “free” replacement of ReLU activation on classification tasks with no performance cost.

We in addition evaluate black box accuracies under transfer attacks using other source and target models. Besides transfer attacks, we also evaluate our method on the state-of-the-art decision-based black box attacks, namely Boundary Attack++ [44]. In these experiments, k -WTA models achieve considerably better robustness against decision-based attacks in comparison to conventional ReLU models. We report the result details in Appendix B.4.

4.3 Loss Landscape in Gradient-Based Attacks

We demonstrate how k -WTA affect the attacker’s loss landscape in gradient-based attacks. Similar to the analysis in [24], we visualize the attack loss of a model with respect to its input on points $x' = x + \epsilon_1 g_1 + \epsilon_2 g_2$, where x is a test sample from CIFAR test set, g_1 is the direction of the loss gradient with respect to the input, g_2 is another random direction, ϵ_1 and ϵ_2 sweep in the range of $[-0.04, 0.04]$, with 50 samples each. This produces a 3D plot with 2500 data points.

As shown in Figure 5, k -WTA models (with $\gamma = 0.1$) have a highly non-convex and non-smooth loss landscape. Thus, the estimated gradient is hardly useful for adversarial searches. This explains why k -WTA models can resist effectively gradient-based attacks. In contrast, ReLU models have a smooth loss surface, from which adversarial samples can be easily found using gradient descent.

Inspecting the range of loss values in Figure 5, we find that adversarial training tends to compress the loss landscape’s dynamic range in both the gradient direction and the other random direction, making the dynamic range smaller than that of the models without adversarial training. This phenomenon has already been observed in ReLU networks [43, 24]. Interestingly, k -WTA models show a similar behavior (Figure 5-a,b). Moreover, we find that in k -WTA models a larger γ leads to a smoother loss surface than a smaller γ (see Appendix B.6 for more details).

5 Conclusion

This paper proposes to replace widely used activation functions with the k -WTA activation for improving the neural network’s robustness against adversarial attacks. This is the only change we advocate. The underlying idea is to embrace the discontinuities introduced by k -WTA functions to make the search for adversarial examples more challenging. Our method comes almost for free, harmless to network training, and readily useful in the current paradigm of neural networks.

References

- [1] Christian Szegedy, Wojciech Zaremba, Ilya Sutskever, Joan Bruna, Dumitru Erhan, Ian Goodfellow, and Rob Fergus. Intriguing properties of neural networks. In *International Conference on Learning Representations*, 2014.
- [2] Marco Barreno, Blaine Nelson, Anthony D Joseph, and J Doug Tygar. The security of machine learning. *Machine Learning*, 81(2):121–148, 2010.
- [3] Marco Barreno, Blaine Nelson, Russell Sears, Anthony D Joseph, and J Doug Tygar. Can machine learning be secure? In *Proceedings of the 2006 ACM Symposium on Information, computer and communications security*, pages 16–25. ACM, 2006.
- [4] Mahmood Sharif, Sruti Bhagavatula, Lujo Bauer, and Michael K. Reiter. Accessorize to a crime: Real and stealthy attacks on state-of-the-art face recognition. In *Proceedings of the 2016 ACM SIGSAC Conference on Computer and Communications Security, CCS '16*, pages 1528–1540, New York, NY, USA, 2016. ACM.
- [5] Simen Thys, Wiebe Van Ranst, and Toon Goedemé. Fooling automated surveillance cameras: adversarial patches to attack person detection. *arXiv preprint arXiv:1904.08653*, 2019.
- [6] Dimitris Tsipras, Shibani Santurkar, Logan Engstrom, Alexander Turner, and Aleksander Madry. Robustness may be at odds with accuracy. *stat*, 1050:11, 2018.
- [7] Hongyang Zhang, Yaodong Yu, Jiantao Jiao, Eric P Xing, Laurent El Ghaoui, and Michael I Jordan. Theoretically principled trade-off between robustness and accuracy. *arXiv preprint arXiv:1901.08573*, 2019.
- [8] Ali Shafahi, W. Ronny Huang, Christoph Studer, Soheil Feizi, and Tom Goldstein. Are adversarial examples inevitable? In *International Conference on Learning Representations*, 2019.
- [9] Dong Su, Huan Zhang, Hongge Chen, Jinfeng Yi, Pin-Yu Chen, and Yupeng Gao. Is robustness the cost of accuracy? – a comprehensive study on the robustness of 18 deep image classification models. In Vittorio Ferrari, Martial Hebert, Cristian Sminchisescu, and Yair Weiss, editors, *Computer Vision – ECCV 2018*, pages 644–661, Cham, 2018. Springer International Publishing.
- [10] Anish Athalye, Nicholas Carlini, and David Wagner. Obfuscated gradients give a false sense of security: Circumventing defenses to adversarial examples. In *Proceedings of the 35th International Conference on Machine Learning, ICML 2018*, July 2018.
- [11] Jacob Buckman, Aurko Roy, Colin Raffel, and Ian Goodfellow. Thermometer encoding: One hot way to resist adversarial examples. 2018.
- [12] Ji Lin, Chuang Gan, and Song Han. Defensive quantization: When efficiency meets robustness. In *International Conference on Learning Representations*, 2019.
- [13] Cihang Xie, Jianyu Wang, Zhishuai Zhang, Zhou Ren, and Alan Yuille. Mitigating adversarial effects through randomization. In *International Conference on Learning Representations*, 2018.
- [14] Chuan Guo, Mayank Rana, Moustapha Cisse, and Laurens van der Maaten. Countering adversarial images using input transformations. In *International Conference on Learning Representations*, 2018.
- [15] Guneet S. Dhillon, Kamyar Aizzadenesheli, Jeremy D. Bernstein, Jean Kossaifi, Aran Khanna, Zachary C. Lipton, and Animashree Anandkumar. Stochastic activation pruning for robust adversarial defense. In *International Conference on Learning Representations*, 2018.
- [16] Jeremy M Cohen, Elan Rosenfeld, and J Zico Kolter. Certified adversarial robustness via randomized smoothing. *arXiv preprint arXiv:1902.02918*, 2019.
- [17] Kaiming He, Xiangyu Zhang, Shaoqing Ren, and Jian Sun. Deep residual learning for image recognition. In *Proceedings of the IEEE conference on computer vision and pattern recognition*, pages 770–778, 2016.
- [18] Gao Huang, Zhuang Liu, Laurens Van Der Maaten, and Kilian Q Weinberger. Densely connected convolutional networks. In *Proceedings of the IEEE conference on computer vision and pattern recognition*, pages 4700–4708, 2017.
- [19] Sergey Zagoruyko and Nikos Komodakis. Wide residual networks. *arXiv preprint arXiv:1605.07146*, 2016.

- [20] Alexey Kurakin, Ian Goodfellow, and Samy Bengio. Adversarial machine learning at scale. *arXiv preprint arXiv:1611.01236*, 2016.
- [21] Seyed-Mohsen Moosavi-Dezfooli, Alhussein Fawzi, and Pascal Frossard. Deepfool: a simple and accurate method to fool deep neural networks. In *Proceedings of the IEEE conference on computer vision and pattern recognition*, pages 2574–2582, 2016.
- [22] Nicholas Carlini and David Wagner. Towards evaluating the robustness of neural networks. In *2017 IEEE Symposium on Security and Privacy (SP)*, pages 39–57. IEEE, 2017.
- [23] Nicolas Papernot, Patrick McDaniel, Ian Goodfellow, Somesh Jha, Z Berkay Celik, and Ananthram Swami. Practical black-box attacks against machine learning. In *Proceedings of the 2017 ACM on Asia conference on computer and communications security*, pages 506–519. ACM, 2017.
- [24] Florian Tramèr, Alexey Kurakin, Nicolas Papernot, Ian Goodfellow, Dan Boneh, and Patrick McDaniel. Ensemble adversarial training: Attacks and defenses. *arXiv preprint arXiv:1705.07204*, 2017.
- [25] Anish Athalye, Logan Engstrom, Andrew Ilyas, and Kevin Kwok. Synthesizing robust adversarial examples. *arXiv preprint arXiv:1707.07397*, 2017.
- [26] Xingjun Ma, Bo Li, Yisen Wang, Sarah M. Erfani, Sudanthi Wijewickrema, Grant Schoenebeck, Michael E. Houle, Dawn Song, and James Bailey. Characterizing adversarial subspaces using local intrinsic dimensionality. In *International Conference on Learning Representations*, 2018.
- [27] Yang Song, Taesup Kim, Sebastian Nowozin, Stefano Ermon, and Nate Kushman. Pixeldefend: Leveraging generative models to understand and defend against adversarial examples. In *International Conference on Learning Representations*, 2018.
- [28] Pouya Samangouei, Maya Kabkab, and Rama Chellappa. Defense-GAN: Protecting classifiers against adversarial attacks using generative models. In *International Conference on Learning Representations*, 2018.
- [29] Stephen Grossberg. Contour enhancement, short term memory, and constancies in reverberating neural networks. In *Studies of mind and brain*, pages 332–378. Springer, 1982.
- [30] E Majani, Ruth Erlanson, and Yaser S Abu-Mostafa. On the k-winners-take-all network. In *Advances in neural information processing systems*, pages 634–642, 1989.
- [31] Wolfgang Maass. Neural computation with winner-take-all as the only nonlinear operation. In *Advances in neural information processing systems*, pages 293–299, 2000.
- [32] Wolfgang Maass. On the computational power of winner-take-all. *Neural computation*, 12(11):2519–2535, 2000.
- [33] Rupesh K Srivastava, Jonathan Masci, Sohrob Kazerounian, Faustino Gomez, and Jürgen Schmidhuber. Compete to compute. In *Advances in Neural Information Processing Systems 26*, pages 2310–2318. 2013.
- [34] Rupesh Kumar Srivastava, Jonathan Masci, Faustino Gomez, and Jürgen Schmidhuber. Understanding locally competitive networks. *arXiv preprint arXiv:1410.1165*, 2014.
- [35] Maximilian Riesenhuber and Tomaso Poggio. Hierarchical models of object recognition in cortex. *Nature neuroscience*, 2(11):1019, 1999.
- [36] Michael McCloskey and Neal J Cohen. Catastrophic interference in connectionist networks: The sequential learning problem. In *Psychology of learning and motivation*, volume 24, pages 109–165. Elsevier, 1989.
- [37] Guido F Montufar, Razvan Pascanu, Kyunghyun Cho, and Yoshua Bengio. On the number of linear regions of deep neural networks. In *Advances in neural information processing systems*, pages 2924–2932, 2014.
- [38] Maithra Raghu, Ben Poole, Jon Kleinberg, Surya Ganguli, and Jascha Sohl Dickstein. On the expressive power of deep neural networks. In *Proceedings of the 34th International Conference on Machine Learning-Volume 70*, pages 2847–2854. JMLR. org, 2017.
- [39] Simon S Du, Xiyu Zhai, Barnabas Poczos, and Aarti Singh. Gradient descent provably optimizes over-parameterized neural networks. *arXiv preprint arXiv:1810.02054*, 2018.
- [40] Yann LeCun, Léon Bottou, Yoshua Bengio, Patrick Haffner, et al. Gradient-based learning applied to document recognition. *Proceedings of the IEEE*, 86(11):2278–2324, 1998.

- [41] Alex Krizhevsky and Geoffrey Hinton. Learning multiple layers of features from tiny images. Technical report, Citeseer, 2009.
- [42] Yuval Netzer, Tao Wang, Adam Coates, Alessandro Bissacco, Bo Wu, and Andrew Y Ng. Reading digits in natural images with unsupervised feature learning. 2011.
- [43] Aleksander Madry, Aleksandar Makelov, Ludwig Schmidt, Dimitris Tsipras, and Adrian Vladu. Towards deep learning models resistant to adversarial attacks. *arXiv preprint arXiv:1706.06083*, 2017.
- [44] Jianbo Chen and Michael I Jordan. Boundary attack++: Query-efficient decision-based adversarial attack. *arXiv preprint arXiv:1904.02144*, 2019.
- [45] Ian J Goodfellow, Jonathon Shlens, and Christian Szegedy. Explaining and harnessing adversarial examples. *arXiv preprint arXiv:1412.6572*, 2014.
- [46] Yinpeng Dong, Fangzhou Liao, Tianyu Pang, Hang Su, Jun Zhu, Xiaolin Hu, and Jianguo Li. Boosting adversarial attacks with momentum. In *Proceedings of the IEEE Conference on Computer Vision and Pattern Recognition*, pages 9185–9193, 2018.
- [47] Wieland Brendel, Jonas Rauber, and Matthias Bethge. Decision-based adversarial attacks: Reliable attacks against black-box machine learning models. *arXiv preprint arXiv:1712.04248*, 2017.
- [48] Jiawei Su, Danilo Vasconcellos Vargas, and Kouichi Sakurai. One pixel attack for fooling deep neural networks. *IEEE Transactions on Evolutionary Computation*, 2019.
- [49] Nina Narodytska and Shiva Prasad Kasiviswanathan. Simple black-box adversarial perturbations for deep networks. *arXiv preprint arXiv:1612.06299*, 2016.
- [50] Ruitong Huang, Bing Xu, Dale Schuurmans, and Csaba Szepesvári. Learning with a strong adversary. <http://arxiv.org/abs/1511.03034>, 11 2015.
- [51] Cihang Xie, Yuxin Wu, Laurens van der Maaten, Alan Yuille, and Kaiming He. Feature denoising for improving adversarial robustness. *arXiv preprint arXiv:1812.03411*, 2018.
- [52] Jia Deng, Wei Dong, Richard Socher, Li-Jia Li, Kai Li, and Li Fei-Fei. Imagenet: A large-scale hierarchical image database. In *2009 IEEE conference on computer vision and pattern recognition*, pages 248–255. Ieee, 2009.
- [53] Andrew Slavin Ross and Finale Doshi-Velez. Improving the adversarial robustness and interpretability of deep neural networks by regularizing their input gradients. *CoRR*, abs/1711.09404, 2017.
- [54] Stephan Zheng, Yang Song, Thomas Leung, and Ian Goodfellow. Improving the robustness of deep neural networks via stability training. In *The IEEE Conference on Computer Vision and Pattern Recognition (CVPR)*, June 2016.
- [55] Jonas Rauber, Wieland Brendel, and Matthias Bethge. Foolbox: A python toolbox to benchmark the robustness of machine learning models. *arXiv preprint arXiv:1707.04131*, 2017.
- [56] Przemyslaw Wojtaszczyk. *Banach spaces for analysts*, volume 25. Cambridge University Press, 1996.

Supplementary Document

Resisting Adversarial Attacks by k -Winners-Take-All

A Other Related Work

In this section, we briefly review the key ideas of attacking neural network models and existing defense methods based on adversarial training.

Attack methods. Recent years have seen adversarial attack studied extensively. The proposed attack methods fall under two general categories, *white-box* and *black-box* attacks.

The white-box threat model assumes that the attacker knows the model’s structure and parameters fully. This means that the attacker can exploit the model’s gradient (with respect to the input) to find adversarial examples. A baseline of such attacks is the *Fast Gradient Sign Method* (FGSM) [45], which constructs the adversarial example \mathbf{x}' of a given labeled data (\mathbf{x}, y) using a gradient-based rule:

$$\mathbf{x}' = \mathbf{x} + \epsilon \text{sign}(\nabla_{\mathbf{x}} L(f(\mathbf{x}), y)), \quad (3)$$

where $f(\mathbf{x})$ denotes the neural network model’s output, $L(\cdot)$ is the loss function provided $f(\mathbf{x})$ and input label y , and ϵ is the perturbation range for the allowed adversarial example.

Extending FGSM, *Projected Gradient Descent* (PGD) [20] utilizes local first-order gradient of the network in a multi-step fashion, and is considered the “strongest” first-order adversary [43]. In each step of PGD, the adversary example is updated by a FGSM rule, namely,

$$\mathbf{x}'_{n+1} = \Pi_{\mathbf{x}' \in \Delta_{\epsilon}} \mathbf{x}'_n + \epsilon \text{sign}(\nabla_{\mathbf{x}} L(f(\mathbf{x}'_n), y)), \quad (4)$$

where \mathbf{x}'_n is the adversary examples after n steps and $\Pi_{\mathbf{x}' \in \Delta_{\epsilon}}(\mathbf{x}'_n)$ projects \mathbf{x}'_n back into an allowed perturbation range Δ_{ϵ} (such as an ϵ ball of \mathbf{x} under certain distance measure). Other attacks include Deepfool [21], C&W [22] and momentum-based attack [46]. Those methods are all using first-order gradient information to construct adversarial samples.

The black-box threat model is a strict subset of the white-box threat model. It assumes that the attacker has no information about the model’s architecture or parameters. Some black-box attack model allows the attacker to query the victim neural network to gather (or reverse-engineer) information. By far the most successful black-box attack is transfer attack [23, 24]. The idea is to first construct adversarial examples on an adversarially trained network and then attack the black-box network model use these samples. There also exist some gradient-free black-box attack methods, such as boundary attack [47, 44], one-pixel attack [48] and local search attack [49]. Those methods rely on repeatedly evaluating the model and are not as effective as gradient-based white-box attacks.

Adversarial training. Adversarial training [45, 43, 20, 50] is by far the most successful method against adversarial attacks. It trains the network model with adversarial images generated during the training time. Madry et al. [43] showed that adversarial training in essence solves the following min-max optimization problem:

$$\min_f \mathbb{E} \{ \max_{\mathbf{x}' \in \Delta_{\epsilon}} L(f(\mathbf{x}'), y) \}, \quad (5)$$

where Δ_{ϵ} is the set of allowed perturbations of training samples, and y denotes the true label of each training sample. Recent works that achieve state-of-the-art adversarial robustness rely on adversarial training [7, 51]. However, adversarial training is notoriously slow because it requires finding adversarial samples on-the-fly at each training epoch. Its prohibitive cost makes adversarial training difficult to scale to large datasets such as ImageNet [52] unless enormous computation resources are available.

Regularization. Another type of defense is based on regularizing the neural network, and many works of this type are combined with adversarial training. For example, *feature denoising* [51] adds several denoise blocks to the network structure and trains the network with adversarial training. Zhang et al. [7] explicitly added a regularization term to balance the trade-off between standard accuracy and robustness, obtaining state-of-the-art robust accuracy on CIFAR.

Some other regularization-based methods require no adversarial training. For example, Ross and Doshi-Velez [53] proposed to regularize the gradient of the model with respect to its input; Zheng

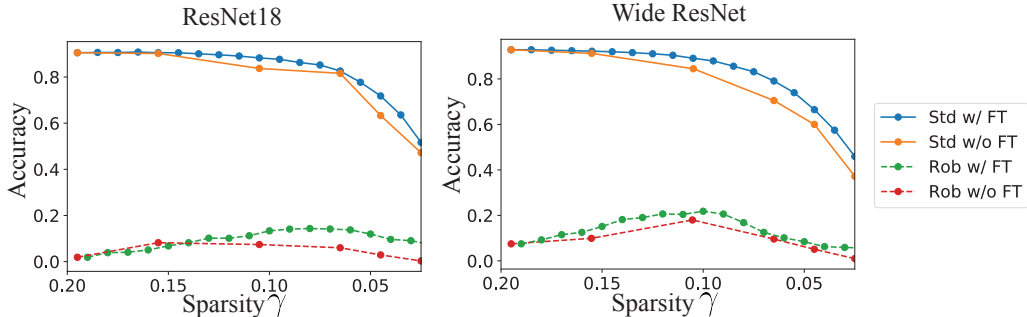


Figure 6: **Efficacy of incremental training.** We sweep through a range of sparsity ratios, and evaluate the standard and robust accuracies of two network structures (left: ResNet18 and right: Wide ResNet). We compare the performance differences between the regular training (i.e., training without incremental fine-tuning) and the training with incremental fine-tuning.

et al. [54] generated adversarial samples by adding random Gaussian noise to input data. However, these methods are shown to be brittle under stronger iterative gradient-based attacks such as PGD [7]. In contrast, as demonstrated in our experiments, our method without using adversarial training is able to greatly improve robustness under PGD and other attacks.

B Additional Experimental Results

B.1 Efficacy of Incremental Training

First, we demonstrate the efficacy of incremental training (described in Sec. 2.2). As shown in Figure 6, models trained with incremental fine-tuning (denoted as w/ FT in the plots’ legend) performs better in terms of both standard accuracy (denoted as `std` in the plots’ legend) and robust accuracy (denoted as `rob` in the plots) when $\gamma < 0.2$, suggesting that fine-tuning is worthwhile when γ is small.

B.2 Complete Results on PGD attack

In Table 4, we report the detailed robustness results for different architectures and attack configurations on CIFAR dataset. The adversarial examples used for *attack tests* are constructed by PGD (for 20 iterations with random initialization). The step size of the PGD attack is $\epsilon/10$, where ϵ is the perturbation size. We experimented with different ϵ values as shown in Table 4

On the other side, the adversarial examples used for *adversarial training* are also constructed by PGD (for 20 iterations with random initialization), with the maximum perturbation range $\epsilon = 8$ (or 0.031 after normalizing pixel values into $[0, 1]$) under ℓ_∞ -norm and a step size of 0.003. All the input images are normalized into $[0, 1]$ before fed into the network.

We find that, after optimized using adversarial training, k -WTA models generally outperform ReLU models that are also optimized with adversarial training. In addition, a wider network (DenseNet, Wide ResNet) performs better than a narrower one—a finding that validates our theoretical analysis in Sec. 3: recall that Theorem 1 states that increasing network width can improve the robustness of k -WTA models.

B.3 Other Gradient-Based Attack

In addition to PGD tests, we also evaluate our method against various other gradient-based attack methods. Our tested attacks include C&W (ℓ_2) [22] attack, Momentum attack [46] and Deepfool [21]. We use Foolbox [55], a third-party toolbox for evaluating adversarial robustness.

In different attack methods, we have the following setups for generating adversarial examples: For C&W (ℓ_2) attack, we set the binary search step to 5, maximum number of iterations to 20, learning rate to 0.01, and initial constant to 0.01. For Deepfool, we use 20 steps and 10 sub-samples in its configuration. For momentum attack, we set the step size to 0.007 and number of iterations to 20. All other parameters are set by Foolbox to be its default values.

Activation	Model	$\epsilon = 0 (A_{std})$	$\epsilon = 1$	$\epsilon = 2$	$\epsilon = 4$	$\epsilon = 8$
ReLU	ResNet18	90.9%	27.2%	5.7%	0.1%	0.00%
ReLU	ResNet18+adv	83.1%	79.5%	74.6%	65.8%	42.9%
ReLU	ResNet18+TRADE	78.9%	76.2%	71.9%	65.8%	50.1%
k -WTA	ResNet18-0.08	85.8%	67.0%	51.3%	30.7%	17.7%
k -WTA	ResNet18-0.08+adv	73.3%	70.7%	68.1%	63.2%	52.4%
k -WTA	ResNet18-0.08+TRADE	70.0%	68.0%	65.2%	61.5%	51.0%
ReLU	DenseNet121	91.1%	13.3%	1.5%	0.0%	0.0%
ReLU	DenseNet121+adv	84.2%	80.0%	75.3%	66.8%	46.1%
k -WTA	DenseNet121-0.09	89.5%	76.9%	58.5%	30.3%	8.8%
k -WTA	DenseNet121-0.09+adv	79.3%	77.2%	76.7%	73.9%	66.2%
ReLU	WideResNet	91.0%	10.1%	0.8%	0.0%	0.0%
ReLU	WideResNet+adv	83.3%	80.0%	75.6%	66.2%	43.1%
k -WTA	WideResNet-0.1	88.6%	74.6%	57.7%	36.0%	22.5%
k -WTA	WideResNet-0.1+adv	73.8%	71.4%	70.0%	66.8%	59.3%

Table 4: Results on CIFAR for different perturbation size ϵ . [Model Name]-0.1 denotes k -WTA model trained with sparsity $\gamma = 0.1$; +adv denotes model trained with adversarial training; +TRADE denotes model trained with TRADE.

Activation	Model	A_{std}	Momentum	Deepfool	C&W
ReLU	ResNet18	88.9%	0.5%	1.0%	0.6%
ReLU	ResNet18+adv	83.1%	54.3%	45.5%	54.7%
k -WTA	ResNet18-0.08	86.1%	32.1%	83.5%	37.5%
k -WTA	ResNet18-0.08+adv	73.3%	53.2%	72.4%	58.7%
k -WTA	ResNet18-0.08+TRADE	70.0%	55.4%	72.4%	60.7%
ReLU	DenseNet121	90.1%	0.2%	0.6%	1.0%
ReLU	DenseNet121+adv	84.2%	52.9%	48.9%	58.8%
k -WTA	DenseNet121-0.09	89.6%	26.2%	88.2%	33.4%
k -WTA	DenseNet121-0.09+adv	79.2%	65.2%	78.2%	65.1%
ReLU	WideResNet	91.1%	0.1%	0.8%	0.1%
ReLU	WideResNet+adv	83.3%	50.0%	49.5%	56.2%
k -WTA	WideResNet-0.1	88.7%	34.1%	85.70%	32.3%
k -WTA	WideResNet-0.1+adv	73.8%	56.8%	71.2%	57.5%

Table 5: Other gradient-based attack on CIFAR.

In all attack methods, we use 2000 adversarial samples to evaluate the robust accuracy of each model. The results on CIFAR and SVHN are listed in Table 5 and Table 6, respectively. The perturbation range of all adversarial samples are clipped into the range $[-0.031, 0.031]$ on CIFAR and the range $[-0.047, 0.047]$ on SVHN (while the image pixel values are normalized in $[0, 1]$). We also find that in some rare cases, other gradient-based attack methods may produce a slightly higher rate of successful attacks than PGD on our k -WTA model, but in general, PGD remains the most effective attack method in our tests.

B.4 Additional Black-Box Attack Results

Transfer attack. We now present the detailed results under transfer attacks in black-box setting on CIFAR (see Table 7) and SVHN (see Table 8). We find that in many transfer attack settings, adversarially trained k -WTA models does not produce better results in comparison to adversarially trained ReLU models. We believe that this is mainly because that k -WTA models with adversarial training usually have slightly lower standard accuracies than ReLU models. We also find that the particular model, k -WTA +DenseNet121-0.09+adv, has its robust accuracy under transfer attack lower than white-box gradient-based attack. While not a general phenomenon, it seems to suggest for this particular model black-box transfer attack is more effective than white-box gradient-based attack. This is possible because our method is particularly motivated for defending against gradient-based attacks. Similar phenomena have been discussed for previous gradient-based defense methods (as pointed out in [10]). In general, the most effective is still the gradient-based attack.

Boundary attack. We use the implementation in Foolbox [55] to generate adversarial samples from Boundary Attack++ [44]. We set the maximum number of evaluations to 1000 while keeping

Model	A_{std}	Momentum	Deepfool	C&W
ResNet18 (Vanilla)	88.9%	0.5%	1.0%	0.6%
ResNet18+adv	83.1%	54.3%	45.5%	54.7%
ResNet18-0.08	86.1%	32.1%	83.5%	37.5%
ResNet18-0.08+adv	80.7%	71.5%	82.3%	75.9%

Table 6: Other gradient-based attack on SVHN

Source Model \ Target Model	ReLU+ResNet18	ReLU+ResNet18+adv	A_{std}
ReLU+ResNet18	5.9%	58.4%	90.9%
ReLU+ResNet18+adv	71.9%	54.1%	73.3%
k -WTA +ResNet18-0.18	41.9%	66.3%	90.6%
k -WTA +ResNet18-0.13	45.6%	66.0%	89.7%
k -WTA +ResNet18-0.08	50.1%	62.0%	86.1%
k -WTA +ResNet18-0.08+adv	50.1%	62.0%	86.1%
ReLU+DenseNet121	6.6%	64.8%	91.1%
ReLU+DenseNet121+adv	81.5%	64.8%	81.5%
k -WTA +DenseNet121-0.18	26.5%	71.7%	92.6%
k -WTA +DenseNet121-0.13	32.1%	70.7%	91.7%
k -WTA +DenseNet121-0.09	37.3%	67.3%	89.5%
k -WTA +DenseNet121-0.09+adv	76.9%	58.3%	79.2%

Table 7: Black-box transfer attack results on CIFAR.

other parameters as their default values. Since the query-based black-box attack is extremely slow, we use only 1000 samples to evaluate the accuracy of each model.

In addition, Athalye et al. [10] argued that obfuscated gradient defense may result in adversarial samples that can be more easily found by brute-force random search. Therefore, we also test our method against random Gaussian noise attack. All attacks are restricted in ℓ_∞ -norm with a perturbation size $\epsilon = 8$ (while the image pixel values are in $[0, 255]$). In the random noise attack, we use 10^3 random samples on each test example. As reported in Table 9, random noise attack is not able to find adversarial examples on either regular models or k -WTA models.

According to our experiments, we find that Boundary Attack++ can effectively reduce the accuracy of a regular ReLU model. But replacing ReLU with k -WTA, even without the expensive adversarial training, significantly improves the robust accuracy, from 19.7% to 66.20% as shown in Table 9. Here k -WTA+adv also has lower robust accuracy than ReLU+adv, mainly because k -WTA+adv in this case has a lower standard accuracy.

B.5 Empirical Worst-Case Robustness

In Table 10, we report the *worst-case* robustness results on all attacking scenarios that we experimented with. Here the worst-case robustness refers to the lowest robust accuracy under all attacks (including both white-box and black-box attacks) we evaluated. As shown in Table 10, k -WTA models with adversarial training always achieve the best performance in comparison to other adversarially trained models—including models trained with TRADE, the state-of-the-art defense method against white-box attacks.

B.6 Loss Landscape Visualization

To help understand how the sparsity ratio γ affects k -WTA’s robustness against gradient-based attacks, we visualize the loss landscapes of k -WTA networks when different sparsity ratios γ are used, and the plots are shown in Figure 7. The way we produce the visualizations is the same as Figure 5 in the main text (see description in Sec. 4.3). As we reasoned in Sec. 3, a larger γ tends to smooth the loss surface of the k -WTA network with respect to the input, while a smaller γ renders the loss surface more discontinuous and “spiky”. In addition, adversarial training tends to reduce the range of the loss values—a similar phenomenon in ReLU networks has already been reported [43, 24]—but that does not mean that the loss surface becomes smoother; the loss surface remains spiky.

Source Model \ Target Model	ReLU+ResNet18	ReLU+ResNet18+adv	A_{std}
ReLU+ResNet18	8.9%	59.2%	92.9%
ReLU+ResNet18+adv	79.3%	77.9%	83.7%
ReLU+ResNet18+TRADE	79.3%	78.5%	86.2%
k -WTA +ResNet18-0.2	13.5%	78.6%	92.3%
k -WTA +ResNet18-0.1	42.4%	75.8%	89.2%
k -WTA +ResNet18-0.07	38.8%	76.4%	88.2%
k -WTA +ResNet18-0.03	49.9%	71.2%	83.5%
k -WTA +ResNet18-0.1+adv	73.3%	73.4%	82.8%

Table 8: Black-box transfer attack results on SVHN.

Attack Method \ Defense Model	Gaussian Noise	Boundary++
ResNet18 (Vanilla)	88.90%	19.70%
ResNet18+adv	83.12%	73.31%
ResNet18-0.08	85.85%	66.20%
ResNet18-0.08+adv	73.30%	67.73%

Table 9: Gaussian noise and Boundary++ black-box attack.

B.7 CNN architecture for MNIST

Lastly, in Table 11, we summarize the CNN architectures that we used in our MNIST experiments reported in Sec. 4.1.

Activation	Model	Dataset	Metric	A_{std}	Worst case A_{rob}	Which attack
ReLU	ResNet18+adv	CIFAR	$l_\infty(0.031)$	83.1%	45.5%	PGD
ReLU	ResNet18+TRADE	CIFAR	$l_\infty(0.031)$	78.9%	50.1%	PGD
k -WTA	ResNet19-0.08+adv	CIFAR	$l_\infty(0.031)$	73.3%	52.4%	PGD
ReLU	DenseNet121+adv	CIFAR	$l_\infty(0.031)$	84.2%	46.1%	PGD
k -WTA	DenseNet121-0.09+adv	CIFAR	$l_\infty(0.031)$	79.3%	58.3%	Transfer attack
ReLU	WideResNet+adv	CIFAR	$l_\infty(0.031)$	83.3%	43.1%	PGD
k -WTA	WideResNet-0.1+adv	CIFAR	$l_\infty(0.031)$	73.8%	56.8%	Momentum
ReLU	ResNet18+adv	SVHN	$l_\infty(0.047)$	84.2%	44.5%	PGD
k -WTA	ResNet18-0.08+adv	SVHN	$l_\infty(0.047)$	80.7%	71.5%	Momentum

Table 10: Empirical worst-case performance evaluation.

Layer	Parameters
Input	size = $1 \times 28 \times 28$
Convolution	output channels=128, kernel size=3, padding=1, stride=1
ReLU/ k -WTA	-
Convolution	output channels=128, kernel size=3, padding=1, stride=2
ReLU/ k -WTA	-
Convolution	output channels=256, kernel size=3, padding=1, stride=1
ReLU/ k -WTA	-
Convolution	output channels=256, kernel size=3, padding=1, stride=2
Linear	input size=12544, output size=10000
ReLU/ k -WTA	-
Linear	input size=10000, output size=10
Softmax output	-

Table 11: MNIST CNN architecture used in Sec. 4.1.

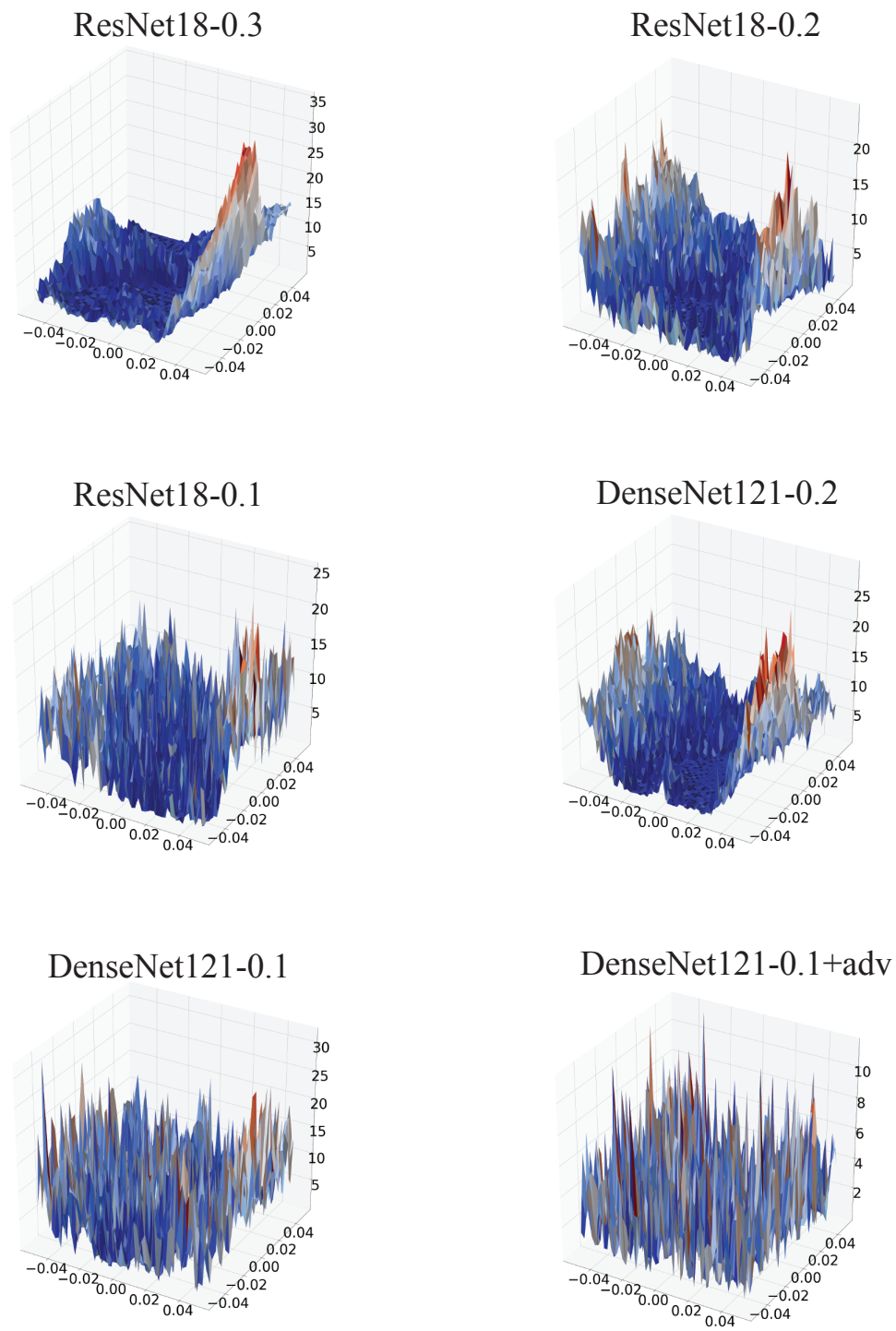


Figure 7: Visualization of different model with different γ .

C Discontinuity Jump of $W\phi_k(x)$

Consider a gradual and smooth change of the vector x . For the ease of illustration, let us assume all the values in x are distinct. Because every element in x changes smoothly, when the activation pattern $\mathcal{A}(x)$ changes, the k -th largest and $k + 1$ -th largest value in x must swap: the previously k -th largest value is removed from the activation pattern, while the previously $k + 1$ -th largest value is added in the activation pattern. Let i and j denote the indices of the two values, that is, x_i is previously the k -th largest and x_j is previously the $k + 1$ -th largest. When this swap happens, x_i and x_j must be infinitesimally close to each other, and we use x^* to indicate their common value.

This swap affects the computation of $W\phi_k(x)$. Before the swap happens, x_i is in the activation pattern but x_j is not, therefore W_i takes effect but W_j does not. After the swap, W_j takes effect while W_i is suppressed. Therefore, the discontinuity jump due to this swap is $(W_j - W_i)x^*$.

When W is determined, the magnitude of the jump depends on x^* . Recall that x^* is the k -th largest value in x when the swap happens. Thus, it depends on k and in turn the sparsity ratio γ : the smaller the γ is, the smaller k is effectively used (for a fixed vector length). As a result, the k -th largest value becomes larger—when $k = 1$, the largest value of x is used as x^* .

D Theoretical Proofs

In this section, we will prove Theorem 1 and Theorem 2. The formal version of the two theorems are Theorem 9 and Theorem 10 respectively.

Notation. We use $[n]$ to denote the set $\{1, 2, \dots, n\}$. We use $\mathbf{1}(\mathcal{E})$ to indicate an indicator variable. If the event \mathcal{E} happens, the value of $\mathbf{1}(\mathcal{E})$ is 1. Otherwise the value of $\mathbf{1}(\mathcal{E})$ is 0. For a weight matrix W , we use W_i to denote the i -th row of W . For a bias vector b , we use b_i to denote the i -th entry of b .

In this section, we show some behaviors of the k -WTA activation function. Recall that an n -layer neural network $f(x)$ with k -WTA activation function can be seen as the following:

$$f(x) = W^{(1)} \cdot \phi_k(W^{(2)} \cdot \phi_k(\dots \phi_k(W^{(n)}x + b^{(n)})) + b^{(2)}) + b^{(1)}$$

where $W^{(i)}$ is the weight matrix, $b^{(i)}$ is the bias vector of the i -th layer, and $\phi(\cdot)$ is the k -WTA activation function, i.e., for an arbitrary vector y , $\phi_k(y)$ is defined as the following:

$$\phi_k(y)_j = \begin{cases} y_j, & \text{if } y_j \text{ is one of the top-}k \text{ largest values,} \\ 0, & \text{otherwise.} \end{cases}$$

For simplicity of the notation, if k is clear in the context, we will just use $\phi(y)$ for short. Notice that if there is a tie in the above definition, we assume the entry with smaller index has larger value. For a vector $y \in \mathbb{R}^l$, we define the activation pattern $\mathcal{A}(y) \subseteq [l]$ as

$$\mathcal{A}(y) = \{i \in [l] \mid y_i \text{ is one of the top-}k \text{ largest values}\}.$$

Notice that if the activation pattern $\mathcal{A}(y)$ is different from $\mathcal{A}(y')$, then $W \cdot \phi(y)$ and $W \cdot \phi(y')$ will be in different linear region. Actually, $W \cdot \phi(y)$ may even represent a discontinuous function. In the next section, we will show that when the network is much wider, the function may be more discontinuous with respect to the input.

D.1 Discontinuity with Respect to the Input

We only consider the activation pattern of the output of one layer. We consider the behavior of the network after the initialization of the weight matrix and the bias vector. By initialization, the entries of the weight matrix W are i.i.d. random Gaussian variables, and the bias vector is zero. We can show that if the weight matrix is sufficiently wide, then for any vector x , with high probability, for all vector x' satisfying that the "perpendicular" distance between x and x' is larger than a small threshold, the activation patterns of Wx and Wx' are different.

Notice that the scaling of W does not change the activation pattern of Wx for any x , we can thus assume that each entry of W is a random variable with standard Gaussian distribution $N(0, 1)$.

Before we prove Theorem 9, let us prove several useful lemmas. The following several lemmas does not depend on the randomness of the weight matrix.

Lemma 1 (Inputs with the same activation pattern form a convex set). *Given an arbitrary weight matrix $W \in \mathbb{R}^{l \times m}$ and an arbitrary bias vector $b \in \mathbb{R}^l$, for any $x \in \mathbb{R}^m$, the set of all the vectors $x' \in \mathbb{R}^m$ satisfying $\mathcal{A}(Wx' + b) = \mathcal{A}(Wx + b)$ is convex, i.e., the set*

$$\{x' \in \mathbb{R}^m \mid \mathcal{A}(Wx + b) = \mathcal{A}(Wx' + b)\}$$

is convex.

Proof. If $\mathcal{A}(Wx' + b) = \mathcal{A}(Wx + b)$, then x' should satisfy:

$$\forall i \in \mathcal{A}(Wx + b), j \in [l] \setminus \mathcal{A}(Wx + b), W_i x' + b_i \geq (\text{or } >) W_j x' + b_j.$$

Notice that the inequality $W_i x' + b_i \geq (\text{or } >) W_j x' + b_j$ denotes a half hyperplane $(W_i - W_j)x' + (b_i - b_j) \geq (\text{or } >) 0$. Thus, the set $\{x' \in \mathbb{R}^m \mid \mathcal{A}(Wx + b) = \mathcal{A}(Wx' + b)\}$ is convex since it is an intersection of half hyperplanes. \square

Lemma 2 (Different patterns of input points with small angle imply different patterns of input points with large angle). *Let $\alpha \in (0, 1)$. Given an arbitrary weight matrix $W \in \mathbb{R}^{l \times m}$, a bias vector $b = 0$, and a vector $x \in \mathbb{R}^m$ with $\|x\|_2 = 1$, if every vector $x' \in \mathbb{R}^m$ with $\|x'\|_2 = 1$ and $\langle x, x' \rangle = \alpha$ satisfies $\mathcal{A}(Wx + b) \neq \mathcal{A}(Wx' + b)$, then for any $x'' \in \mathbb{R}^m$ with $\|x''\|_2 = 1$ and $\langle x, x'' \rangle < \alpha$, it satisfies $\mathcal{A}(Wx + b) \neq \mathcal{A}(Wx'' + b)$.*

Proof. We draw a line between x and x'' . There must be a point $x^* \in \mathbb{R}^m$ on the line and $\langle x, x^* \rangle = \alpha$, where $x^* = x^*/\|x^*\|_2$. Since $b = 0$, we have $\mathcal{A}(Wx^* + b) = \mathcal{A}(Wx' + b) \neq \mathcal{A}(Wx + b)$. Since x^* is on the line between x and x'' , we have $\mathcal{A}(Wx'' + b) \neq \mathcal{A}(Wx + b)$ by convexity (see Lemma 1). \square

Lemma 3 (A sufficient condition for different patterns). *Consider two vectors $y \in \mathbb{R}^l$ and $y' \in \mathbb{R}^l$. If $\exists i \in \mathcal{A}(y), j \in [l] \setminus \mathcal{A}(y)$ such that $y'_i < y'_j$, then $\mathcal{A}(y) \neq \mathcal{A}(y')$.*

Proof. Suppose $\mathcal{A}(y) = \mathcal{A}(y')$. We have $i \in \mathcal{A}(y')$. It means that y'_i is one of the top- k largest values among all entries of y' . Thus y'_j is also one of the top- k largest values, and j should be in $\mathcal{A}(y')$ which leads to a contradiction. \square

In the remaining parts, we will assume that each entry of the weight matrix $W \in \mathbb{R}^{l \times m}$ is a standard random Gaussian variable.

Lemma 4 (Upper bound of the entires of W). *Consider a matrix $W \in \mathbb{R}^{l \times m}$ where each entry is a random variable with standard Gaussian distribution $N(0, 1)$. With probability at least 0.99, $\forall i \in [l]$, $\|W_i\|_2 \leq 10\sqrt{ml}$.*

Proof. Consider a fixed $i \in [l]$. We have $\mathbb{E}[\|W_i\|_2^2] = m$. By Markov's inequality, we have $\Pr[\|W_i\|_2^2 > 100ml] \leq 0.01/l$. By taking union bound over all $i \in [l]$, with probability at least 0.99, we have $\forall i \in [l], \|W_i\|_2 \leq 10\sqrt{ml}$. \square

Lemma 5 (Two vectors may have different activation patterns with a good probability). *Consider a matrix $W \in \mathbb{R}^{l \times m}$ where each entry is a random variable with standard Gaussian distribution $N(0, 1)$. Let $\gamma \in (0, 0.48)$ be the sparsity ratio of the activation, i.e., $\gamma = k/l$. For any two vectors $x, x' \in \mathbb{R}^m$ with $\|x\|_2 = \|x'\|_2 = 1$ and $\langle x, x' \rangle = \alpha$ for some arbitrary $\alpha \in (0.5, 1)$, with probability at least $1 - 2^{-\Theta((1/\alpha^2 - 1)\gamma^l)}$, $\mathcal{A}(Wx) \neq \mathcal{A}(Wx')$ and $\exists i \in \mathcal{A}(Wx), j \in [l] \setminus \mathcal{A}(Wx)$ such that*

$$W_i x' < W_j x' - \frac{\sqrt{1 - \alpha^2}}{24\alpha} \cdot \sqrt{2\pi}.$$

Proof. Consider arbitrary two vectors $x, x' \in \mathbb{R}^m$ with $\|x\|_2 = \|x'\|_2 = 1$ and $\langle x, x' \rangle = \alpha$. We can find an orthogonal matrix $Q \in \mathbb{R}^{m \times m}$ such that $\tilde{x} := Qx = (1, 0, 0, \dots, 0)^\top \in \mathbb{R}^m$ and $\tilde{x}' := Qx' = (\alpha, \sqrt{1 - \alpha^2}, 0, 0, \dots, 0)^\top \in \mathbb{R}^m$. Let $\tilde{W} = WQ^\top$. Then we have $\tilde{W}\tilde{x} = Wx$ and $\tilde{W}\tilde{x}' = Wx'$. Thus, we only need to analyze the activation patterns of $\tilde{W}\tilde{x}$ and $\tilde{W}\tilde{x}'$. Since Q^\top is an orthogonal matrix and each entry of W is an i.i.d. random variable with standard Gaussian distribution $N(0, 1)$, $\tilde{W} = WQ^\top$ is also a random matrix where each entry is an i.i.d. random

variable with standard Gaussian distribution $N(0, 1)$. Let the entries in the first column of \tilde{W} be X_1, X_2, \dots, X_l and let the entries in the second column of \tilde{W} be Y_1, Y_2, \dots, Y_l . Then we have

$$Wx = \tilde{W}\tilde{x} = \begin{pmatrix} X_1 \\ X_2 \\ \dots \\ X_l \end{pmatrix}, \quad Wx' = \tilde{W}\tilde{x}' = \begin{pmatrix} \alpha X_1 + \sqrt{1 - \alpha^2} Y_1 \\ \alpha X_2 + \sqrt{1 - \alpha^2} Y_2 \\ \dots \\ \alpha X_l + \sqrt{1 - \alpha^2} Y_l \end{pmatrix}. \quad (6)$$

We set $\varepsilon = \sqrt{1 - \alpha^2}/(96\alpha)$ and define $R'_1 < R_1 < R_2 < R'_2$ as follows:

$$\Pr_{X \sim N(0,1)} [X \geq R'_2] = (1 - 2\varepsilon)\gamma, \quad (7)$$

$$\Pr_{X \sim N(0,1)} [X \geq R_2] = (1 - \varepsilon)\gamma, \quad (8)$$

$$\Pr_{X \sim N(0,1)} [X \geq R_1] = (1 + \varepsilon)\gamma, \quad (9)$$

$$\Pr_{X \sim N(0,1)} [X \geq R'_1] = (1 + 2\varepsilon)\gamma. \quad (10)$$

Since $\gamma < 0.48$ and $\varepsilon \leq 0.02$, we have $(1 + 2\varepsilon)\gamma < 0.5$. It implies $0 < R'_1 < R_1 < R_2 < R'_2$.

Claim 3.

$$R'_2 - R'_1 \leq 8\varepsilon\sqrt{2\pi}.$$

Proof. By Equation (7) and Equation (10),

$$\Pr_{X \sim N(0,1)} [R'_1 \leq X \leq R'_2] = 4\varepsilon\gamma.$$

Due to the density function of standard Gaussian distribution, we have

$$\frac{1}{\sqrt{2\pi}} \int_{R'_1}^{R'_2} e^{-t^2/2} dt = \Pr_{X \sim N(0,1)} [R'_1 \leq X \leq R'_2] = 4\varepsilon\gamma.$$

Since $R'_2 \geq R'_1 \geq 0$, we have $\forall t \in [R'_1, R'_2]$, $e^{-t^2/2} \geq e^{-R_2'^2/2}$. Thus,

$$\frac{1}{\sqrt{2\pi}} \cdot e^{-R_2'^2/2} (R'_2 - R'_1) = \frac{1}{\sqrt{2\pi}} \cdot e^{-R_2'^2/2} \int_{R'_1}^{R'_2} 1 dt \leq \frac{1}{\sqrt{2\pi}} \int_{R'_1}^{R'_2} e^{-t^2/2} dt = 4\varepsilon\gamma.$$

By the tail bound of Gaussian distribution, we have

$$\Pr_{X \sim N(0,1)} [X \geq R'_2] \leq e^{-R_2'^2/2}.$$

By combining with Equation (7), we have

$$\begin{aligned} & (1 - 2\varepsilon)\gamma \cdot \frac{1}{\sqrt{2\pi}} (R'_2 - R'_1) \\ &= \Pr_{X \sim N(0,1)} [X \geq R'_2] \cdot \frac{1}{\sqrt{2\pi}} (R'_2 - R'_1) \\ &\leq e^{-R_2'^2/2} \cdot \frac{1}{\sqrt{2\pi}} (R'_2 - R'_1) \\ &\leq 4\varepsilon\gamma, \end{aligned}$$

which implies

$$R'_2 - R'_1 \leq \frac{4\varepsilon}{1 - 2\varepsilon} \sqrt{2\pi} \leq 8\varepsilon\sqrt{2\pi},$$

where the last inequality follows from $1 - 2\varepsilon \geq 0.5$. \square

Claim 4.

$$\Pr_{X_1, X_2, \dots, X_l} \left[\sum_{i=1}^l \mathbf{1}(X_i \geq R_2) \geq (1 - \varepsilon/2)\gamma l \right] \leq e^{-\varepsilon^2 \gamma l / 24} \quad (11)$$

$$\Pr_{X_1, X_2, \dots, X_l} \left[\sum_{i=1}^l \mathbf{1}(X_i \geq R_1) \leq (1 + \varepsilon/2)\gamma l \right] \leq e^{-\varepsilon^2 \gamma l / 18} \quad (12)$$

$$\Pr_{X_1, X_2, \dots, X_l} \left[\sum_{i=1}^l \mathbf{1}(R'_2 \geq X_i \geq R_2) \leq \varepsilon \gamma l / 2 \right] \leq e^{-\varepsilon \gamma l / 8} \quad (13)$$

$$\Pr_{X_1, X_2, \dots, X_l} \left[\sum_{i=1}^l \mathbf{1}(R_1 \geq X_i \geq R'_1) \leq \varepsilon \gamma l / 2 \right] \leq e^{-\varepsilon \gamma l / 8} \quad (14)$$

Proof. For $i \in [l]$, we have $\mathbb{E}[\mathbf{1}(X_i \geq R_2)] = \Pr[X_i \geq R_2] = (1 - \varepsilon)\gamma$ by Equation (8). By Chernoff bound, we have

$$\Pr \left[\sum_{i=1}^l \mathbf{1}(X_i \geq R_2) \geq (1 + \varepsilon/2) \cdot (1 - \varepsilon)\gamma l \right] \leq e^{-(\varepsilon/2)^2 (1 - 2\varepsilon)\gamma l / 3}.$$

Since $\varepsilon \leq 0.02$,

$$\Pr \left[\sum_{i=1}^l \mathbf{1}(X_i \geq R_2) \geq (1 - \varepsilon/2)\gamma l \right] \leq e^{-\varepsilon^2 \gamma l / 24}.$$

We have $\mathbb{E}[\mathbf{1}(X_i \geq R_1)] = \Pr[X_i \geq R_1] = (1 + \varepsilon)\gamma$ by Equation (9). By Chernoff bound, we have

$$\Pr \left[\sum_{i=1}^l \mathbf{1}(X_i \geq R_1) \leq (1 - \varepsilon/3) \cdot (1 + \varepsilon)\gamma l \right] \leq e^{-(\varepsilon/3)^2 (1 + \varepsilon)\gamma l / 2}.$$

Thus,

$$\Pr \left[\sum_{i=1}^l \mathbf{1}(X_i \geq R_i) \leq (1 + \varepsilon/2)\gamma l \right] \leq e^{-\varepsilon^2 \gamma l / 18}$$

We have $\mathbb{E}[\mathbf{1}(R'_2 \geq X_i \geq R_2)] = \Pr[R'_2 \geq X_i \geq R_2] = \varepsilon\gamma$ by Equation (7) and Equation (8). By Chernoff bound, we have

$$\Pr \left[\sum_{i=1}^l \mathbf{1}(R'_2 \geq X_i \geq R_2) \leq 1/2 \cdot \varepsilon \gamma l \right] \leq e^{-\varepsilon \gamma l / 8}$$

Similarly, we have $\mathbb{E}[\mathbf{1}(R_1 \geq X_i \geq R'_1)] = \Pr[R_1 \geq X_i \geq R'_1] = \varepsilon\gamma$ by Equation (9) and Equation (10). By Chernoff bound, we have

$$\Pr_{X_1, X_2, \dots, X_l} \left[\sum_{i=1}^l \mathbf{1}(R_1 \geq X_i \geq R'_1) \leq 1/2 \cdot \varepsilon \gamma l \right] \leq e^{-\varepsilon \gamma l / 8}$$

□

Equation (11) says that, with high probability, $\forall i \in [l]$ with $X_i \geq R_2$, it has $i \in \mathcal{A}(Wx)$. Equation (12) says that, with high probability, $\forall i \in [l]$ with $X_i \leq R_1$, it has $i \notin \mathcal{A}(Wx)$. Equation (14) (Equation (13)) says that, with high probability, there are many $i \in [l]$ such that $W_i x \in [R'_1, R_1]$ ($W_i x \in [R_2, R'_2]$).

Let $\mathcal{E} = \mathcal{E}_1 \wedge \mathcal{E}_2 \wedge \mathcal{E}_3 \wedge \mathcal{E}_4$, where

- $\mathcal{E}_1: \sum_{i=1}^l \mathbf{1}(X_i \geq R_2) \leq (1 - \varepsilon/2)\gamma l$,
- $\mathcal{E}_2: \sum_{i=1}^l \mathbf{1}(X_i \geq R_1) \geq (1 + \varepsilon/2)\gamma l$,

- $\mathcal{E}_3: \sum_{i=1}^l \mathbf{1}(R_1 \geq X_i \geq R'_1) \geq \varepsilon\gamma l/2$,
- $\mathcal{E}_4: \sum_{i=1}^l \mathbf{1}(R'_2 \geq X_i \geq R_2) \geq \varepsilon\gamma l/2$.

According to Equation (11), Equation (12), Equation (13) and Equation (14), the probability that \mathcal{E} happens is at least

$$1 - 4e^{-\varepsilon^2\gamma l/24} \quad (15)$$

by union bound over $\bar{\mathcal{E}}_1, \bar{\mathcal{E}}_2, \bar{\mathcal{E}}_3, \bar{\mathcal{E}}_4$.

Claim 5. *Condition on \mathcal{E} , the probability that $\exists i \in [l]$ with $X_i \in [R_2, R'_2]$ such that $Y_i < -\alpha/\sqrt{1-\alpha^2} \cdot 16\varepsilon\sqrt{2\pi}$ is at least*

$$1 - \left(16\varepsilon \cdot \frac{\alpha}{\sqrt{1-\alpha^2}} + \frac{1}{2}\right)^{\varepsilon\gamma l/2}.$$

Proof. For a fixed $i \in [l]$,

$$\begin{aligned} \Pr \left[Y_i \geq -\alpha/\sqrt{1-\alpha^2} \cdot 16\varepsilon\sqrt{2\pi} \right] &= \int_{-\alpha/\sqrt{1-\alpha^2} \cdot 16\varepsilon\sqrt{2\pi}}^0 \frac{1}{\sqrt{2\pi}} e^{-t^2/2} dt + \frac{1}{2} \\ &\leq \frac{1}{\sqrt{2\pi}} \cdot \alpha/\sqrt{1-\alpha^2} \cdot 16\varepsilon\sqrt{2\pi} + \frac{1}{2} \\ &= 16\varepsilon \cdot \frac{\alpha}{\sqrt{1-\alpha^2}} + \frac{1}{2}. \end{aligned}$$

Thus, according to event \mathcal{E}_4 , we have

$$\Pr \left[\forall i \text{ with } X_i \in [R_2, R'_2], Y_i \geq -\alpha/\sqrt{1-\alpha^2} \cdot 16\varepsilon\sqrt{2\pi} \mid \mathcal{E} \right] \leq \left(16\varepsilon \cdot \frac{\alpha}{\sqrt{1-\alpha^2}} + \frac{1}{2}\right)^{\varepsilon\gamma l/2}.$$

□

Claim 6. *Condition on \mathcal{E} , the probability that $\exists i \in [l]$ with $X_i \in [R'_1, R_1]$ such that $Y_i \geq 0$ is at least $1 - (1/2)^{\varepsilon\gamma l/2}$.*

Proof. For a fixed $i \in [l]$, $\Pr[Y_i \leq 0] = 1/2$. Thus, according to event \mathcal{E}_3 , we have

$$\Pr [\forall i \text{ with } X_i \in [R'_1, R_1], Y_i \leq 0 \mid \mathcal{E}] \leq (1/2)^{\varepsilon\gamma l/2}.$$

□

Condition on that \mathcal{E} happens. Because of \mathcal{E}_1 , if $X_i \geq R_2$, X_i must be one of the top- k largest values. Due to Equation (6), we have $X_i = W_i x$. Thus, if $X_i \geq R_2$, $i \in \mathcal{A}(Wx)$. By Claim 5, with probability at least

$$1 - \left(16\varepsilon \cdot \frac{\alpha}{\sqrt{1-\alpha^2}} + \frac{1}{2}\right)^{\varepsilon\gamma l/2}, \quad (16)$$

there is $i \in \mathcal{A}(Wx)$ such that

$$\begin{aligned} W_i x' &= \alpha X_i + \sqrt{1-\alpha^2} Y_i \\ &\leq \alpha X_i + \sqrt{1-\alpha^2} \cdot \left(-\frac{\alpha}{\sqrt{1-\alpha^2}} \cdot 16\varepsilon\sqrt{2\pi}\right) \\ &= \alpha(X_i - 16\varepsilon\sqrt{2\pi}) \\ &\leq \alpha(R'_2 - 16\varepsilon\sqrt{2\pi}), \end{aligned} \quad (17)$$

where the first step follows from Equation (6), the second step follows from $Y_i \leq -\alpha/\sqrt{1-\alpha^2} \cdot 16\varepsilon\sqrt{2\pi}$, and the last step follows from $X_i \in [R_2, R'_2]$.

Because of \mathcal{E}_2 if $X_j \leq R_1$, X_j should not be one of the top- k largest values. Due to Equation (6), we have $X_j = W_j x$. Thus, if $X_j \leq R_1$, $j \notin \mathcal{A}(Wx)$. By Claim D.1, with probability at least

$$1 - (1/2)^{\varepsilon\gamma l/2}, \quad (18)$$

there is $j \notin \mathcal{A}(Wx)$ such that

$$W_j x' = \alpha X_j + \sqrt{1 - \alpha^2} Y_j \geq \alpha X_j \geq \alpha R_1, \quad (19)$$

where the first step follows from Equation (6), the second step follows from $Y_j \geq 0$, and the last step follows from $X_j \in [R_1', R_1]$.

By Equation (19) and Equation (17), $\exists i \in \mathcal{A}(Wx), j \in [l] \setminus \mathcal{A}(Wx)$,

$$\begin{aligned} W_i x' &\leq \alpha(R_2' - 16\varepsilon\sqrt{2\pi}) \leq \alpha(R_1' - 8\varepsilon\sqrt{2\pi}) \leq W_j x' - 8\alpha\varepsilon\sqrt{2\pi} \\ &\leq W_j x' - 4\varepsilon\sqrt{2\pi} = W_j x' - \frac{\sqrt{1 - \alpha^2}}{24\alpha} \cdot \sqrt{2\pi}, \end{aligned}$$

where the second step follows from Claim 3, the fourth step follows from $\alpha \geq 0.5$, and the last step follows from $\varepsilon = \sqrt{1 - \alpha^2}/(96\alpha)$. By Lemma 3, we can conclude $\mathcal{A}(Wx) \neq \mathcal{A}(Wx')$. By Equation (15), Equation (16), Equation (18), and union bound, the overall probability is at least

$$\begin{aligned} &1 - \left(4e^{-\varepsilon^2\gamma l/24} + \left(16\varepsilon \cdot \frac{\alpha}{\sqrt{1 - \alpha^2}} + \frac{1}{2} \right)^{\varepsilon\gamma l/2} + \left(\frac{1}{2} \right)^{\varepsilon\gamma l/2} \right) \\ &\geq 1 - \left(4e^{-\varepsilon^2\gamma l/24} + \left(\frac{2}{3} \right)^{\varepsilon\gamma l/2} + \left(\frac{1}{2} \right)^{\varepsilon\gamma l/2} \right) \\ &\geq 1 - 6 \cdot \left(\frac{2}{3} \right)^{\varepsilon^2\gamma l/24} \\ &\geq 1 - 2^{-\Theta\left(\left(\frac{1}{\alpha^2} - 1\right)\gamma l\right)}, \end{aligned}$$

where the first and the last step follows from $\varepsilon = \sqrt{1 - \alpha^2}/(96\alpha)$ \square

Next, we will use a tool called ε -net.

Definition 7 (ε -Net). *For a given set \mathcal{S} , if there is a set $\mathcal{N} \subseteq \mathcal{S}$ such that $\forall x \in \mathcal{S}$ there exists a vector $y \in \mathcal{N}$ such that $\|x - y\|_2 \leq \varepsilon$, then \mathcal{N} is an ε -net of \mathcal{S} .*

There is a standard upper bound of the size of an ε -net of a unit norm ball.

Lemma 6 ([56] II.E, 10). *Given a matrix $U \in \mathbb{R}^{m \times d}$, let $\mathcal{S} = \{Uy \mid \|Uy\|_2 = 1\}$. For $\varepsilon \in (0, 1)$, there is an ε -net \mathcal{N} of \mathcal{S} with $|\mathcal{N}| \leq (1 + 1/\varepsilon)^d$.*

Now we can extend above lemma to the following.

Lemma 7 (ε -Net for the set of points with a certain angle). *Given a vector $x \in \mathbb{R}^m$ with $\|x\|_2 = 1$ and a parameter $\alpha \in (-1, 1)$, let $\mathcal{S} = \{x' \in \mathbb{R}^m \mid \|x'\|_2 = 1, \langle x, x' \rangle = \alpha\}$. For $\varepsilon \in (0, 1)$, there is an ε -net \mathcal{N} of \mathcal{S} with $|\mathcal{N}| \leq (1 + 1/\varepsilon)^{m-1}$.*

Proof. Let $U \in \mathbb{R}^{m \times (m-1)}$ have orthonormal columns and $Ux = 0$. Then \mathcal{S} can be represented as

$$\mathcal{S} = \{\alpha \cdot x + \sqrt{1 - \alpha^2} \cdot Uy \mid y \in \mathbb{R}^{m-1}, \|Uy\|_2 = 1\}.$$

Let

$$\mathcal{S}' = \{Uy \mid y \in \mathbb{R}^{m-1}, \|Uy\|_2 = 1\}.$$

According to Lemma 6, there is an ε -net \mathcal{N}' of \mathcal{S}' with size $|\mathcal{N}'| \leq (1 + 1/\varepsilon)^{m-1}$. We construct \mathcal{N} as following:

$$\mathcal{N} = \{\alpha \cdot x + \sqrt{1 - \alpha^2} \cdot z \mid z \in \mathcal{N}'\}.$$

It is obvious that $|\mathcal{N}| = |\mathcal{N}'| \leq (1 + 1/\varepsilon)^{m-1}$. Next, we will show that \mathcal{N} is indeed an ε -net of \mathcal{S} . Let x' be an arbitrary vector from \mathcal{S} . Let $x' = \alpha \cdot x + \sqrt{1 - \alpha^2} \cdot z$ for some $z \in \mathcal{S}'$. There is a vector $(\alpha \cdot x + \sqrt{1 - \alpha^2} \cdot z') \in \mathcal{N}$ such that $z' \in \mathcal{N}'$ and $\|z - z'\|_2 \leq \varepsilon$. Thus, we have

$$\|x' - (\alpha \cdot x + \sqrt{1 - \alpha^2} \cdot z')\|_2 = \sqrt{1 - \alpha^2} \|z - z'\|_2 \leq \varepsilon. \quad \square$$

Theorem 8 (Rotating a vector a little bit may change the activation pattern). *Consider a weight matrix $W \in \mathbb{R}^{l \times m}$ where each entry is an i.i.d. sample drawn from the Gaussian distribution $N(0, 1/l)$. Let $\gamma \in (0, 0.48)$ be the sparsity ratio of the activation function, i.e., $\gamma = k/l$. With probability at least 0.99, it has $\forall i \in [l], \|W_i\|_2 \leq 10\sqrt{m}$. Condition on that $\forall i \in [l], \|W_i\|_2 \leq 10\sqrt{m}$ happens, then, for any $x \in \mathbb{R}^m$ and $\alpha \in (0.5, 1)$, if*

$$l \geq C \cdot \left(\frac{m + \log(1/\delta)}{\gamma} \cdot \frac{1}{1 - \alpha^2} \right) \cdot \log \left(\frac{m + \log(1/\delta)}{\gamma} \cdot \frac{1}{1 - \alpha^2} \right)$$

for a sufficiently large constant C , with probability at least $1 - \delta \cdot 2^{-m}$, $\forall x' \in \mathbb{R}^m$ with $\frac{\langle x, x' \rangle}{\|x\|_2 \|x'\|_2} \leq \alpha$, $\mathcal{A}(Wx) \neq \mathcal{A}(Wx')$.

Proof. Notice that the scale of W does not affect the activation pattern of Wx for any $x \in \mathbb{R}^m$. Thus, we assume that each entry of W is a standard Gaussian random variable in the remaining proof, and we will instead condition on $\forall i \in [l], \|W_i\|_2 \leq 10\sqrt{ml}$. The scale of x or x' will not affect $\frac{\langle x, x' \rangle}{\|x\|_2 \|x'\|_2}$. It will not affect the activation pattern either. Thus, we assume $\|x\|_2 = \|x'\|_2 = 1$.

By Lemma 4, with probability at least 0.99, we have $\forall i \in [l], \|W_i\|_2 \leq 10\sqrt{ml}$.

Let

$$\mathcal{S} = \{y \in \mathbb{R}^m \mid \|y\|_2 = 1, \langle x, y \rangle = \alpha\}.$$

Set

$$\varepsilon = \frac{\sqrt{2\pi(1 - \alpha^2)}}{720\alpha\sqrt{ml}}.$$

By Lemma 7, there is an ε -net \mathcal{N} of \mathcal{S} such that

$$|\mathcal{N}| \leq \left(1 + \frac{720\alpha\sqrt{ml}}{\sqrt{2\pi(1 - \alpha^2)}} \right)^m.$$

By Lemma 5, for any $y \in \mathcal{N}$, with probability at least

$$1 - 2^{-\Theta((1/\alpha^2 - 1)\gamma l)},$$

$\exists i \in \mathcal{A}(Wx), j \in [l] \setminus \mathcal{A}(Wx)$ such that

$$W_i y < W_j y - \frac{\sqrt{1 - \alpha^2}}{24\alpha} \cdot \sqrt{2\pi}.$$

By taking union bound over all $y \in \mathcal{N}$, with probability at least

$$\begin{aligned} & 1 - |\mathcal{N}| \cdot 2^{-\Theta((1/\alpha^2 - 1)\gamma l)} \\ & \geq 1 - \left(1 + \frac{720\alpha\sqrt{ml}}{\sqrt{2\pi(1 - \alpha^2)}} \right)^m 2^{-\Theta((\frac{1}{\alpha^2} - 1)\gamma l)} \\ & \geq 1 - \left(1000 \cdot \frac{\sqrt{ml}}{\sqrt{1 - \alpha^2}} \right)^m 2^{-\Theta((\frac{1}{\alpha^2} - 1)\gamma l)} \\ & \geq 1 - \left(1000 \cdot \frac{\sqrt{ml}}{\sqrt{1 - \alpha^2}} \right)^m 2^{-C' \cdot (\frac{1}{\alpha^2} - 1)\gamma \cdot \frac{m + \log(1/\delta)}{\gamma} \cdot \frac{\alpha^2}{1 - \alpha^2} \cdot \log\left(\frac{ml}{1 - \alpha^2}\right)} \quad // C' \text{ is a sufficiently large constant} \\ & = 1 - \left(1000 \cdot \frac{\sqrt{ml}}{\sqrt{1 - \alpha^2}} \right)^m 2^{-C' \cdot (m + \log(1/\delta)) \cdot \log\left(\frac{ml}{1 - \alpha^2}\right)} \\ & \geq 1 - \delta \cdot 2^{-m}, \end{aligned}$$

the following event \mathcal{E}' happens: $\forall y \in \mathcal{N}, \exists i \in \mathcal{A}(Wx), j \in [l] \setminus \mathcal{A}(Wx)$ such that

$$W_i y < W_j y - \frac{\sqrt{1 - \alpha^2}}{24\alpha} \cdot \sqrt{2\pi}.$$

In the remaining of the proof, we will condition on the event \mathcal{E}' . Consider $y' \in \mathcal{S}$. Since \mathcal{N} is an ε -net of \mathcal{S} , we can always find a $y \in \mathcal{N}$ such that

$$\|y - y'\|_2 \leq \varepsilon = \frac{\sqrt{2\pi(1-\alpha^2)}}{720\alpha\sqrt{ml}}.$$

Since event \mathcal{E}' happens, we can find $i \in \mathcal{A}(Wx)$ and $j \in [l] \setminus \mathcal{A}(Wx)$ such that

$$W_i y < W_j y - \frac{\sqrt{1-\alpha^2}}{24\alpha} \cdot \sqrt{2\pi}.$$

Then, we have

$$\begin{aligned} W_i y' &= W_i y + W_i(y' - y) \\ &< W_j y - \frac{\sqrt{1-\alpha^2}}{24\alpha} \cdot \sqrt{2\pi} + \|W_i\|_2 \|y' - y\|_2 \\ &\leq W_j y - \frac{\sqrt{1-\alpha^2}}{24\alpha} \cdot \sqrt{2\pi} + 10\sqrt{ml} \cdot \frac{\sqrt{2\pi(1-\alpha^2)}}{720\alpha\sqrt{ml}} \\ &= W_j y - \frac{\sqrt{1-\alpha^2}}{36\alpha} \cdot \sqrt{2\pi} \\ &= W_j y' + W_j(y - y') - \frac{\sqrt{1-\alpha^2}}{36\alpha} \cdot \sqrt{2\pi} \\ &\leq W_j y' + \|W_j\|_2 \|y - y'\|_2 - \frac{\sqrt{1-\alpha^2}}{36\alpha} \cdot \sqrt{2\pi} \\ &\leq W_j y' + 10\sqrt{ml} \cdot \frac{\sqrt{2\pi(1-\alpha^2)}}{720\alpha\sqrt{ml}} - \frac{\sqrt{1-\alpha^2}}{36\alpha} \cdot \sqrt{2\pi} \\ &\leq W_j y' - \frac{\sqrt{1-\alpha^2}}{72\alpha} \cdot \sqrt{2\pi}, \end{aligned}$$

where the second step follows from $W_i y < W_j y - \sqrt{1-\alpha^2}/(24\alpha) \cdot \sqrt{2\pi}$ and $W_i(y' - y) \leq \|W_i\|_2 \|y' - y\|_2$, the third step follows from $\|W_i\|_2 \leq 10\sqrt{ml}$ and $\|y' - y\|_2 \leq \sqrt{2\pi(1-\alpha^2)}/(720\alpha\sqrt{ml})$, the sixth step follows from $W_j(y - y') \leq \|W_j\|_2 \|y - y'\|_2$, and the seventh step follows from $\|W_i\|_2 \leq 10\sqrt{ml}$ and $\|y' - y\|_2 \leq \sqrt{2\pi(1-\alpha^2)}/(720\alpha\sqrt{ml})$.

By Lemma 3, we know that $\mathcal{A}(Wx) \neq \mathcal{A}(Wy')$. Thus, $\forall y' \in \mathbb{R}^m$ with $\|y'\|_2 = 1$ and $\langle x, y' \rangle = \alpha$, we have $\mathcal{A}(Wx) \neq \mathcal{A}(Wy')$ conditioned on \mathcal{E}' . By Lemma 2, we can conclude that $\forall x' \in \mathbb{R}^m$ with $\|x'\|_2 = 1$ and $\langle x, x' \rangle \leq \alpha$, we have $\mathcal{A}(Wx) \neq \mathcal{A}(Wx')$ conditioned on \mathcal{E}' . \square

Theorem 9 (A formal version of Theorem 1). *Consider a weight matrix $W \in \mathbb{R}^{l \times m}$ where each entry is an i.i.d. sample drawn from the Gaussian distribution $N(0, 1/l)$. Let $\gamma \in (0, 0.48)$ be the sparsity ratio of the activation function, i.e., $\gamma = k/l$. With probability at least 0.99, it has $\forall i \in [l], \|W_i\|_2 \leq 10\sqrt{m}$. Condition on that $\forall i \in [l], \|W_i\|_2 \leq 10\sqrt{m}$ happens, then, for any $x \in \mathbb{R}^m$, if*

$$l \geq C \cdot \left(\frac{m + \log(1/\delta)}{\gamma} \cdot \frac{1}{\beta} \right) \cdot \log \left(\frac{m + \log(1/\delta)}{\gamma} \cdot \frac{1}{\beta} \right)$$

for some $\beta \in (0, 1)$ and a sufficiently large constant C , with probability at least $1 - \delta \cdot 2^{-m}$, $\forall x' \in \mathbb{R}^m$ with $\|\Delta x\|_2^2 / \|x\|_2^2 \geq \beta$, $\mathcal{A}(Wx) \neq \mathcal{A}(Wx')$, where $x' = c \cdot (x + \Delta x)$ for some scalar c , and Δx is perpendicular to x .

Proof. If $\langle x, x' \rangle \leq 0$, then the statement follows from Theorem 8 directly. In the following, we consider the case $\langle x, x' \rangle > 0$. If $\|\Delta x\|_2/\|x\|_2^2 \geq \beta$,

$$\begin{aligned} & \frac{\langle x, x' \rangle^2}{\|x\|_2^2 \|x'\|_2^2} \\ &= \frac{c^2 \|x\|_2^4}{\|x\|_2^2 (c^2 (\|x\|_2^2 + \|\Delta x\|_2^2))} \\ &= \frac{\|x\|_2^2}{\|x\|_2^2 + \|\Delta x\|_2^2} \\ &\leq \frac{\|x\|_2^2}{\|x\|_2^2 + \beta \|x\|_2^2} \\ &\leq \frac{1}{1 + \beta}. \end{aligned}$$

Thus,

$$\frac{1}{1 - \frac{\langle x, x' \rangle^2}{\|x\|_2^2 \|x'\|_2^2}} \leq \frac{1}{\beta} + 1 \leq O\left(\frac{1}{\beta}\right).$$

By Theorem 8, we conclude the proof. \square

Example 1. Suppose that the training data contains N points $x_1, x_2, \dots, x_N \in \mathbb{R}^m$ ($m \geq \Omega(\log N)$), where each entry of x_i for $i \in [N]$ is an i.i.d. Bernoulli random variable, i.e., each entry is 1 with some probability $p \in (100 \log(N)/m, 0.5)$ and 0 otherwise. Consider a weight matrix $W \in \mathbb{R}^{l \times m}$ where each entry is an i.i.d. sample drawn from the Gaussian distribution $N(0, 1/l)$. Let $\gamma \in (0, 0.48)$ be the sparsity ratio of the activation function, i.e., $\gamma = k/l$. If $l \geq \Omega(m/\gamma \cdot \log(m/\gamma))$, then with probability at least 0.9, $\forall i, j \in [N]$, the activation pattern of $W x_i$ and $W x_j$ are different, i.e., $\mathcal{A}(W x_i) \neq \mathcal{A}(W x_j)$.

Proof. Firstly, let us bound $\|x_i\|_2$. We have $\mathbb{E}[\|x_i\|_2^2] = \mathbb{E}[\sum_{t=1}^m x_{i,t}] = pm$. By Bernstein inequality, we have

$$\Pr \left[\left| \sum_{t=1}^m x_{i,t} - pm \right| > \frac{1}{10} pm \right] \leq 2e^{-\frac{(pm/10)^2/2}{pm + \frac{1}{3} \cdot \frac{1}{10} pm}} \leq 0.01/N.$$

Thus, by taking union bound over all $i \in [N]$, with probability at least 0.99, $\forall i \in [N]$, $\sqrt{0.9pm} \leq \|x_i\|_2 \leq \sqrt{1.1pm}$.

Next we consider $\langle x_i, x_j \rangle$. Notice that $\mathbb{E}[\langle x_i, x_j \rangle] = \mathbb{E}[\sum_{t=1}^m x_{i,t} x_{j,t}] = p^2 m$. There are two cases.

Case 1 ($p^2 m > 20 \log N$). By Bernstein inequality, we have

$$\Pr \left[\left| \langle x_i, x_j \rangle - p^2 m \right| > \frac{1}{2} p^2 m \right] \leq 2e^{-\frac{(p^2 m/2)^2/2}{p^2 m + \frac{1}{3} \cdot \frac{1}{2} p^2 m}} = 2e^{-\frac{3}{28} p^2 m} \leq 0.01/N^2.$$

By taking union bound over all pairs of i, j , with probability at least 0.99, $\forall i \neq j$, $\langle x_i, x_j \rangle \leq \frac{3}{2} p^2 m$. Since $\|x_i\|_2, \|x_j\|_2 \geq \sqrt{0.9pm}$, we have

$$\frac{\langle x_i, x_j \rangle}{\|x_i\|_2 \|x_j\|_2} \leq \frac{3p^2 m/2}{0.9pm} = \frac{5}{3} p \leq \frac{5}{6}.$$

Case 2 ($p^2 m \leq 20 \log N$). By Bernstein inequality, we have

$$\Pr \left[\left| \langle x_i, x_j \rangle - p^2 m \right| > 10 \log N \right] \leq 2e^{-\frac{(10 \log N)^2/2}{p^2 m + \frac{1}{3} \cdot 10 \log N}} \leq 0.01/N^2.$$

By taking union bound over all pairs of i, j , with probability at least 0.99, $\forall i \neq j$, $\langle x_i, x_j \rangle \leq 10 \log N$. Since $\|x_i\|_2, \|x_j\|_2 \geq \sqrt{0.9pm} \geq \sqrt{90 \log N}$, we have

$$\frac{\langle x_i, x_j \rangle}{\|x_i\|_2 \|x_j\|_2} \leq \frac{10 \log N}{90 \log N} = \frac{1}{9}.$$

Thus, with probability at least 0.98, we have $\forall i \neq j, \langle x_i, x_j \rangle / (\|x_i\|_2 \|x_j\|_2) \leq 5/6$. By Theorem 8, with probability at least 0.99, $\forall q \in [l], \|W_q\|_2 \leq 10\sqrt{m}$. Condition on this event, and since $\forall i \neq j$ we have $\langle x_i, x_j \rangle / (\|x_i\|_2 \|x_j\|_2) \leq 5/6$, by Theorem 8 again and union bound over all $i \in [N]$, with probability at least 0.99, $\forall i \neq j, \mathcal{A}(Wx_i) \neq \mathcal{A}(Wx_j)$. \square

D.2 Disjointness of Activation Patterns of Different Input Points

Let X_1, X_2, \dots, X_m be i.i.d. random variables drawn from the standard Gaussian distribution $N(0, 1)$. Let $Z = \sum_{i=1}^m X_i^2$. We use the notation χ_m^2 to denote the distribution of Z . If m is clear in the context, we just use χ^2 for short.

Lemma 8 (A property of χ^2 distribution). *Let Z be a random variable with χ_m^2 ($m \geq 2$) distribution. Given arbitrary $\varepsilon, \eta \in (0, 1)$, if R is sufficiently large then*

$$\Pr[Z \geq (1 + \varepsilon)R] / \Pr[(1 + \varepsilon)R \geq Z \geq R] \leq \eta.$$

Proof. Let R be a sufficiently large number such that:

- $e^{\varepsilon R/2} \geq \frac{4}{\varepsilon}$.
- $e^{\varepsilon R/8} \geq R^{m/2-1}$.
- $e^{\varepsilon R/4} \geq \frac{16}{9} \cdot \frac{1}{\eta}$.

Let $\xi = \varepsilon/4$. By the density function of χ^2 distribution, we have

$$\Pr[R \leq Z \leq (1 + \varepsilon)R] = \frac{1}{2^{m/2}\Gamma(m/2)} \int_R^{(1+\varepsilon)R} t^{m/2-1} e^{-t/2} dt,$$

and

$$\Pr[Z \geq (1 + \varepsilon)R] = \frac{1}{2^{m/2}\Gamma(m/2)} \int_{(1+\varepsilon)R}^{\infty} t^{m/2-1} e^{-t/2} dt,$$

where $\Gamma(\cdot)$ is the Gamma function, and for integer $m/2$, $\Gamma(m/2) = (m/2 - 1)(m/2 - 2) \cdots 2 \cdot 1 = (m/2 - 1)!$. By our choice of R , we have

$$\begin{aligned} \Pr[R \leq Z \leq (1 + \varepsilon)R] &\geq \frac{1}{2^{m/2}\Gamma(m/2)} \int_R^{(1+\varepsilon)R} e^{-t/2} dt \\ &= \frac{1}{2^{m/2}\Gamma(m/2)} \cdot 2 \left(e^{-R/2} - e^{-(1+\varepsilon)R/2} \right) \\ &\geq \frac{1}{2^{m/2}\Gamma(m/2)} \cdot 2(1 - \xi) \cdot e^{-R/2}, \end{aligned}$$

where the first step follows from $\forall t \geq R, t^{m/2-1} \geq 1$, and the third step follows from

$$\frac{e^{-(1+\varepsilon)R/2}}{e^{-R/2}} = e^{-\varepsilon R/2} \leq \xi.$$

We also have:

$$\begin{aligned} \Pr[Z \geq (1 + \varepsilon)R] &\leq \frac{1}{2^{m/2}\Gamma(m/2)} \int_{(1+\varepsilon)R}^{+\infty} e^{-(1-\xi)t/2} dt \\ &= \frac{1}{2^{m/2}\Gamma(m/2)} \cdot \frac{2}{1 - \xi} \cdot e^{-(1-\xi)(1+\varepsilon)R/2} \\ &\leq \frac{1}{2^{m/2}\Gamma(m/2)} \cdot \frac{2}{1 - \xi} \cdot e^{-(1+\varepsilon/2)R/2}, \end{aligned}$$

where the first step follows from $\forall t \geq R, t^{m/2-1} \leq e^{\xi t/2}$, and the third step follows from $(1 - \xi)(1 + \varepsilon) \geq (1 + \varepsilon/2)$.

Thus, we have

$$\frac{\Pr[Z \geq (1 + \varepsilon)R]}{\Pr[(1 + \varepsilon)R \geq Z \geq R]} \leq \frac{1}{(1 - \xi)^2} e^{-\varepsilon R/4} \leq \frac{16}{9} e^{-\varepsilon R/4} \leq \eta.$$

\square

Lemma 9. Consider $x, y, z \in \mathbb{R}^m$. If $\frac{\langle x, y \rangle}{\|x\|_2 \|y\|_2} \leq \alpha$, $\frac{\langle x, z \rangle}{\|x\|_2 \|z\|_2} \geq \beta$ for some $\alpha, \beta \geq 0$, then $\frac{\langle y, z \rangle}{\|y\|_2 \|z\|_2} \leq \alpha + \sqrt{1 - \beta^2}$. Furthermore, if $\beta = \frac{2 + \alpha + \sqrt{2 - \alpha^2}}{4}$, then $\frac{\langle y, z \rangle}{\|y\|_2 \|z\|_2} \leq (1 - \varepsilon_\alpha)\beta$, where $\varepsilon_\alpha \in (0, 1)$ only depends on α .

Proof. Without loss of generality, we suppose $\|x\|_2 = \|y\|_2 = \|z\|_2 = 1$. We can decompose y as $ax + y'$ where y' is perpendicular to x . We can decompose z as $b_1x + b_2y'/\|y'\|_2 + z'$ where z' is perpendicular to both x and y' . Then we have:

$$\langle y, z \rangle = ab_1 + b_2\|y'\|_2 \leq \alpha + \sqrt{1 - \beta^2},$$

where the last inequality follows from $0 \leq b_1 \leq 1, a \leq \alpha$, and $b_2 \leq \sqrt{1 - b_1^2} \leq \sqrt{1 - \beta^2}$, $0 \leq \|y'\|_2 \leq 1$.

By solving $\beta \geq \alpha + \sqrt{1 - \beta^2}$, we can get $\beta \geq \frac{\alpha + \sqrt{2 - \alpha^2}}{2}$. Thus, if we set

$$\beta = \frac{1 + \frac{\alpha + \sqrt{2 - \alpha^2}}{2}}{2},$$

β should be strictly larger than $\alpha + \sqrt{1 - \beta^2}$, and the gap only depends on α . \square

Lemma 10. Give $x \in \mathbb{R}^m$, let $y \in \mathbb{R}^m$ be a random vector, where each entry of y is an i.i.d. sample drawn from the standard Gaussian distribution $N(0, 1)$. Given $\beta \in (0.5, 1)$, $\Pr[\langle x, y \rangle / (\|x\|_2 \|y\|_2) \geq \beta] \geq 1 / (1 + 1 / \sqrt{2(1 - \beta)})^m$.

Proof. Without loss of generality, we can assume $\|x\|_2 = 1$. Let $y' = y / \|y\|_2$. Since each entry of y is an i.i.d. Gaussian variable, y' is a random vector drawn uniformly from a unit sphere. Notice that if $\langle x, y' \rangle \geq \beta$, then $\|x - y'\|_2 \leq \sqrt{2(1 - \beta)}$. Let $C = \{z \in \mathbb{R}^m \mid \|z\|_2 = 1, \|z - x\|_2 \leq \sqrt{2(1 - \beta)}\}$ be a cap, and let $\mathcal{S} = \{z \in \mathbb{R}^m \mid \|z\|_2 = 1\}$ be the unit sphere. Then we have

$$\Pr[\langle x, y' \rangle \geq \beta] = \text{area}(C) / \text{area}(\mathcal{S}).$$

According to Lemma 6, there is an $\sqrt{2(1 - \beta)}$ -net \mathcal{N} with $|\mathcal{N}| \leq (1 + 1 / \sqrt{2(1 - \beta)})^m$. If we put a cap centered at each point in \mathcal{N} , then the whole unit sphere will be covered. Thus, we can conclude

$$\Pr[\langle x, y' \rangle \geq \beta] \geq 1 / (1 + 1 / \sqrt{2(1 - \beta)})^m. \quad \square$$

Theorem 10 (A formal version of Theorem 2). Consider N data points $x_1, x_2, \dots, x_N \in \mathbb{R}^m$ and a weight matrix $W \in \mathbb{R}^{l \times m}$ where each entry of W is an i.i.d. sample drawn from the Gaussian distribution $N(0, 1/l)$. Suppose $\forall i \neq j \in [N], \langle x_i, x_j \rangle / (\|x_i\|_2 \|x_j\|_2) \leq \alpha$ for some $\alpha \in (0.5, 1)$. Fix $k \geq 1$ and $\delta \in (0, 1)$, if l is sufficiently large, then with probability at least $1 - \delta$,

$$\forall i, j \in [N], \mathcal{A}(Wx_i) \cap \mathcal{A}(Wx_j) = \emptyset.$$

Proof. Notice that the scale of W and x_1, x_2, \dots, x_N do not affect either $\langle x_i, x_j \rangle / (\|x_i\|_2 \|x_j\|_2)$ or the activation pattern. Thus, we can assume $\|x_1\|_2 = \|x_2\|_2 = \dots = \|x_N\|_2 = 1$ and each entry of W is an i.i.d. standard Gaussian random variable.

Let $\beta = \frac{2 + \alpha + \sqrt{2 - \alpha^2}}{4}$ and ε_α be the same as mentioned in Lemma 9. Set ε and β' as

$$\varepsilon = \frac{\frac{1}{\beta} - 1}{2}, \quad \beta' = (1 + \varepsilon)\beta.$$

Set

$$\eta = \frac{\delta/100}{100k \log(N/\delta) \cdot (1 + 2/\sqrt{2(1 - \beta')})^m}.$$

Let R satisfies

$$\Pr_{Z \sim \chi_m^2} [Z \geq (1 + \varepsilon)^2 R^2] = \frac{\delta/100}{l}.$$

Due to Lemma 8, if l is sufficiently large, then R is sufficiently large such that

$$\Pr_{Z \sim \chi_m^2} [Z \geq (1 + \varepsilon)^2 R^2] / \Pr_{Z \sim \chi_m^2} [(1 + \varepsilon)^2 R^2 \geq Z \geq R^2] \leq \eta.$$

Notice that for $t \in [l]$, $\|W_t\|_2^2$ is a random variable with χ_m^2 distribution. Thus, $\Pr[\|W_t\|_2 \geq (1 + \varepsilon)R] = \frac{\delta/100}{l}$. By taking union bound over all $t \in [l]$, with probability at least $1 - \delta/100$, $\forall t \in [l]$, $\|W_t\|_2 \leq (1 + \varepsilon)R$. In the remaining of the proof, we will condition on that $\forall t \in [l]$, $\|W_t\|_2 \leq (1 + \varepsilon)R$. Consider $i, j \in [N]$, $t \in [l]$, if $W_t x_i > \beta' R$, then we have

$$\frac{W_t x_i}{\|W_t\|_2} > \frac{\beta' R}{(1 + \varepsilon)R} \geq \beta' / (1 + \varepsilon) = \beta.$$

Due to Lemma 9, we have

$$\frac{W_t x_j}{\|W_t\|_2} < (1 - \varepsilon_\alpha)\beta.$$

Thus,

$$W_t x_j < (1 - \varepsilon_\alpha)\beta \|W_t\|_2 \leq (1 - \varepsilon_\alpha)\beta(1 + \varepsilon)R \leq (1 - \varepsilon_\alpha)\beta' R. \quad (20)$$

Notice that for $i \in [N]$, $t \in [l]$, we have

$$\begin{aligned} \Pr[W_t x_i > \beta' R] &\geq \Pr[\|W_t\|_2 \geq R] \Pr\left[\frac{W_t x_i}{\|W_t\|_2} \geq \beta'\right] \\ &\geq \frac{\delta/100}{l} \cdot \frac{1}{\eta} \cdot \frac{1}{(1 + 1/\sqrt{2(1 - \beta')})^m} \\ &\geq \frac{1}{l} \cdot 100k \log(N/\delta). \end{aligned}$$

By Chernoff bound, with probability at least $1 - \delta/(100N)$,

$$\sum_{t=1}^l \mathbf{1}(W_t x_i > \beta' R) \geq k.$$

By taking union bound over $i \in [N]$, with probability at least $1 - \delta/100$, $\forall i \in [N]$,

$$\sum_{t=1}^l \mathbf{1}(W_t x_i > \beta' R) \geq k.$$

This implies that $\forall i \in [N]$, if $t \in \mathcal{A}(W x_i)$, then $W_t x_i > \beta' R$. Due to Equation (20), $\forall j \in [N]$, we have $W_t x_j < \beta' R$ which implies that $t \notin \mathcal{A}(W x_j)$. Thus, with probability at least $1 - \delta/50 \geq 1 - \delta$ probability, $\forall i \neq j$, $\mathcal{A}(W x_i) \cap \mathcal{A}(W x_j) = \emptyset$. \square

Remark 1. Consider any $x_1, x_2, \dots, x_N \in \mathbb{R}^m$ with $\|x_1\|_2 = \|x_2\|_2 = \dots = \|x_N\|_2 = 1$. If $\forall i \neq j \in [N]$, $\langle x_i, x_j \rangle \leq \alpha$ for some $\alpha \in (0.5, 1)$, then $|N| \leq (1 + 2/\sqrt{2(1 - \alpha)})^m$.

Proof. Since $\langle x_i, x_j \rangle \leq \alpha$, $\|x_i - x_j\|_2^2 = \|x_i\|_2^2 + \|x_j\|_2^2 - 2\langle x_i, x_j \rangle \geq 2 - 2\alpha$. Let \mathcal{S} be the unit sphere, i.e., $\mathcal{S} = \{x \in \mathbb{R}^m \mid \|x\|_2 = 1\}$. Due to Lemma 6, there is a $(\sqrt{2(1 - \alpha)}/2)$ -net \mathcal{N} of \mathcal{S} with size at most $|\mathcal{N}| \leq (1 + 2/\sqrt{2(1 - \alpha)})^m$. Consider x_i, x_j , and $y \in \mathcal{N}$. By triangle inequality, if $\|x_i - y\|_2 < \sqrt{2(1 - \alpha)}/2$, then $\|x_j - y\|_2 > \sqrt{2(1 - \alpha)}/2$ due to $\|x_i - x_j\|_2 \geq \sqrt{2(1 - \alpha)}$. Since \mathcal{N} is a net of \mathcal{S} , for each x_i , we can find a $y \in \mathcal{N}$ such that $\|x_i - y\|_2 < \sqrt{2(1 - \alpha)}/2$. Thus, we can conclude $N \leq |\mathcal{N}| \leq (1 + 2/\sqrt{2(1 - \alpha)})^m$. \square

Theorem 11. Consider N data points $x_1, x_2, \dots, x_N \in \mathbb{R}^m$ with their corresponding labels $z_1, z_2, \dots, z_N \in \mathbb{R}$ and a weight matrix $W \in \mathbb{R}^{l \times m}$ where each entry of W is an i.i.d. sample drawn from the Gaussian distribution $N(0, 1/l)$. Suppose $\forall i \neq j \in [N]$, $\langle x_i, x_j \rangle / (\|x_i\|_2 \|x_j\|_2) \leq \alpha$ for some $\alpha \in (0.5, 1)$. Fix $k \geq 1$ and $\delta \in (0, 1)$, if l is sufficiently large, then with probability at least $1 - \delta$, there exists a vector $v \in \mathbb{R}^l$ such that

$$\forall i \in [N], \langle v, \phi_k(W x_i) \rangle = z_i.$$

Proof. Due to Theorem 10, with probability at least $1 - \delta$, $\forall i \neq j$, $\mathcal{A}(Wx_i) \cap \mathcal{A}(Wx_j) = \emptyset$. Let $t_1, t_2, \dots, t_N \in [l]$ such that $t_i \in \mathcal{A}(Wx_i)$. Then $t_i \notin \mathcal{A}(Wx_j)$ for $j \neq i$.

For each entry v_t , if $t = t_i$ for some $i \in [N]$, then set $v_t = z_i / (W_t x_i)$. Then for $i \in [N]$, we have

$$\langle v, \phi_k(Wx_i) \rangle = \sum_{t \in \mathcal{A}(Wx_i)} v_t \cdot W_t x_i = z_i / (W_{t_i} x_i) \cdot W_{t_i} x_i = z_i.$$

□